

NTIA Report 00-380

**Flexible Interoperable Transceiver (FIT) Program
Test Range I: Radio Propagation Measurements at
440, 1360, and 1920 MHZ
Edwards Air Force Base, CA**

**Peter Papazian
Perry Wilson
Michael Cotton
Yeh Lo**



**U.S. DEPARTMENT OF COMMERCE
Norman Y. Mineta, Secretary**

Gregory L. Rohde, Assistant Secretary
for Communications and Information

October 2000

This Page Intentionally Left Blank

This Page Intentionally Left Blank

Disclaimer

Certain commercial equipment and materials are identified in this report to specify adequately the technical aspects of the reported results. In no case does such identification imply recommendations or endorsement by the National Telecommunications and Information Administration, nor does it imply that the material or equipment identified is the best available for this purpose.

This Page Intentionally Left Blank

This Page Intentionally Left Blank

CONTENTS

EXECUTIVE SUMMARY.....	vii
LIST OF FIGURES.....	xi
LIST OF TABLES.....	xiv
ABSTRACT	1
1. INTRODUCTION	1
2. SITE DESCRIPTION	2
3. MEASUREMENT SYSTEM	3
4. BASIC TRANSMISSION LOSS	5
5. DELAY STATISTICS	9
6. REFERENCES	13
7. FIGURES	14
APPENDIX A: ANTENNA CALIBRATIONS	41
APPENDIX B: EIRP AND ANTENNA GAIN.....	47

This Page Intentionally Left Blank

This Page Intentionally Left Blank

EXECUTIVE SUMMARY

This report describes mobile communication link measurements made at Edwards Air Force Base, CA as part of the Flexible Interoperable Transceiver (FIT) program. Edwards Air Force Base (EAFB) is the first of four locations to be measured, the other three being Fort Hood TX, Fort Polk, LA and Camp Lejeune, NC. The goal of the measurement series is to define communication link characteristics at different frequencies over a representative cross section of military installations.

The measurements were made using the ITS multiple channel impulse response system (see Report, Section 3). The primary figures of merit used to characterize wireless communication links are basic transmission loss (L_{BT}) and delay statistics. Three frequencies are considered: 440 MHz, 1360 MHz, and 1920 MHz. 440 MHz is representative of several current ground-to-ground communication links (JRTC-IS, PRIME, PLRS). 1360 MHz is proposed for the next generation FIT system. 1920 MHz has similar characteristics to the 1710-1850 MHz band, which is also under consideration for FIT. By comparing the 1360 MHz and 1920 MHz basic transmission loss and delay statistics to those for 440 MHz, the viability of using higher frequencies for future military communications and the associated system requirements can be assessed.

For this study two transmitter sites were chosen. Site 1 was located near the flight line and hangars. The ground elevation at this site was 701 m and the transmitter antennas were at a height of 706 m. This site was chosen to simulate a low, close in transmitter, in the clutter of the flight-line buildings. Such a site might be used to communicate with aircraft on the flight line and personnel and data terminals near the flight line buildings. Site 2 was placed on the roof of the AF-38 radar site on a prominent hill. Ground elevation at the site is 805 m and the transmitter antennas were at an elevation of 809 m. This site was chosen as representative of an optimum transmitter site for long range communication (see Report, Section 2).

Data were collected simultaneously at three frequencies along multiple drive routes (short range, long range). This allowed a direct comparison of basic transmission loss and delay statistics in several representative environments. The major question answered by the survey are the effects of frequency translation on these radio propagation parameters. To quantify propagation impairments caused by frequency translation, the impulse response data were analyzed and the following metrics tabulated:

1. Linear curve fit parameters n (path loss exponent) and B (multiplier) are tabulated for basic transmission loss (L_{BT}) versus distance for three frequencies. This data is summarized in tables ES1-ES4. The path loss exponent, n , is the critical parameter. For line-of-sight propagation with free space loss (L_{FS}), $n = 2$ (for example, see Cell 2 Route 2, Figure 4.4). In areas with obstructions caused by terrain, vegetation, or buildings n typically varies between 2 and 4 due to multipath interference (see Cell 1 Route 1, Figure 4.1). Full shadowing can cause the path loss to be more or less independent of distance (D) and results in loss exponents less than 2 (see Cell 2 Route 1, Figure 4.3). Column one in Tables ES1 through ES4 shows the n and B parameters

(see Report, Section 4 for more details). By substituting these parameters into the curve fit equation a best fit approximation of path loss versus distance can be calculated for the different frequencies and routes. These curves then are used in conjunction with the free space loss curve to determine additional loss over free space ($\Delta L_{BT/FS}$) for specific transmitters and routes. They also are used to determine signal loss due to frequency translation from 440 MHz to higher frequencies ($\Delta L_{BT/440}$).

2. $\Delta L_{BT/FS}$ is used to designate the difference between the linear fit to the measured basic transmission loss and ideal free space values. These data then indicate the additional loss over the basic free space loss for the measured frequencies. The $\Delta L_{BT/FS}$ data range is approximately 20 to 40 (dB) for Cell 1 (low transmitter) and 10 to 20 (dB) for Cell 2 (high transmitter). The lower differences for Cell 2 indicate the better line of sight coverage for the high transmitter site. Tables ES1 through ES4 and Report Section 4 give these data at multiple distances.
3. The difference between the 1360 and 1920 MHz linear fit estimates and the 440 MHz linear fit estimate is designated $\Delta L_{BT/440}$. These numbers can be used to determine the extra transmit power, system sensitivity, diversity gain, or BER versus signal-to-noise requirements of the proposed higher frequency systems. The $\Delta L_{BT/440}$ data range over approximately 5 to 15 dB for the 1360 MHz data and 10 to 20 dB for the 1920 MHz data (see Tables ES1 through ES4 and Report, Section 4).
4. An alternative to curve fitting the measured data is to bin the L_{BT} data. This is done versus distance and the mean, and standard deviation for each bin are calculated as well as the 90% and 99% probability levels (i.e. 99% of the L_{BT} data are less than this level). 99% L_{BT} levels range from 126 to 163 dB in Cell 1 and from 117 to 157 dB in Cell 2. These data give the upper bounds for the measured transmission loss, L_{BT} , and indicate maximum signal loss on the link required to ensure a certain channel availability probability (see Tables ES5 and ES6 and Report, Section 4). The difference between the mean and the 99% level also can be added to the curve fit to extend the curve fit requirements to the 99% availability level.
5. Delay statistics are necessary for design of a digital system. They are used to determine equalizer requirements for elimination of inter-symbol interference. In general, delay increases with frequency and with the presence of scattering objects (low transmitter). Two figures of merit are the delay spread and the maximum delay. At 90% probability, the maximum delay ranges from 8.7 μ s (low transmitter, long-range route) down to 5.6 μ s (high transmitter, long range route) for 440 MHz and from 19.0 μ s down to 7.7 μ s for 1920 MHz. These data are based on a 20 dB interval of discrimination (impulse peak to noise > 23 dB, only echoes within 20 dB of the peak are included in the statistics). For a 10-dB interval of discrimination and 90% probability, the maximum delays reduce from 5.2 to 0.2 μ s and from 10.5 to 0.5 μ s for 440 and 1920 MHz respectively for low and high transmitters and long routes. The delay spreads are up to 2.2 μ s for 440 MHz and up to 4.1 μ s for 1920 MHz (see Report, Section 5 for more details). In addition, impulse data can be used through simulation to determine the optimum equalizer design.

Table ES1. Curve Fit Parameters, Free Space Loss and 440 MHz Loss Compared to Basic Transmission Loss Data, Cell 1 Route 1 (Low Transmitter, Short-Range Route)

F (MHz)	L_{BT} Linear Fit Parameters		D 0.7 km		
	n	B (km^{-1})	L_{FS} (dB)	$\Delta L_{BT/FS}$ (dB)	$\Delta L_{BT/440}$ (dB)
440	3.8	9.0e+2	82.2	24.2	0.0
1360	3.1	9.1e+3	92.0	26.0	11.6
1920	4.1	1.0e+3	95.0	21.9	10.5

Table ES2. Curve Fit Parameters, Free Space Loss and 440 MHz Loss Compared to Basic Transmission Loss Data, Cell 1 Route 2 (Low Transmitter, Long-Range Route)

F (MHz)	L_{BT} Linear Fit Parameters		D					
			3.0 km			8.0 km		
	n	B (km^{-1})	L_{FS} (dB)	$\Delta L_{BT/FS}$ (dB)	$\Delta L_{BT/440}$ (dB)	L_{FS} (dB)	$\Delta L_{BT/FS}$ (dB)	$\Delta L_{BT/440}$ (dB)
440	1.9	1.6e+6	94.9	31.9	0.0	103.4	31.5	0.0
1360	4.6	2.5e+2	104.7	27.2	5.1	113.2	38.3	16.6
1920	3.9	1.1e+3	104.7	29.8	10.7	116.2	37.8	19.2

Table ES3. Curve Fit Parameters, Free Space Loss and 440 MHz Loss Compared to Basic Transmission Loss Data, Cell 2 Route 1 (High Transmitter, Short-Range Route)

F (MHz)	L_{BT} Linear Fit Parameters		D					
			4.5 km			6.5 km		
	n	B (km^{-1})	L_{FS} (dB)	$\Delta L_{BT/FS}$ (dB)	$\Delta L_{BT/440}$ (dB)	L_{FS} (dB)	$\Delta L_{BT/FS}$ (dB)	$\Delta L_{BT/440}$ (dB)
440	0.7*	3.3e+15	98.4	14.9	0.0	101.6	12.8	0.0
1360	0.9*	4.8e+13	108.2	20.8	15.7	111.4	19.0	16.1
1920	1.0*	4.5e+12	111.2	21.8	19.8	114.4	20.2	20.2

* values lower than free space are due to shadowing

Table ES4. Basic Transmission Loss, L_{BT} , Data for Cell 2 Route 2 (High Transmitter, Long-Range Route)

F (MHz)	L_{BT} Linear Fit Parameters		D					
			2.0 km			20.0 km		
	n	B (km^{-1})	L_{FS} (dB)	$\Delta L_{BT/FS}$ (dB)	$\Delta L_{BT/440}$ (dB)	L_{FS} (dB)	$\Delta L_{BT/FS}$ (dB)	$\Delta L_{BT/440}$ (dB)
440	2.1	4.5e+4	91.3	12.8	0.0	111.3	13.8	0.0
1360	1.9	1.1e+6	101.1	19.1	16.2	121.1	18.1	14.2
1920	1.7	2.8e+6	104.1	10.7	10.7	124.1	7.7	6.7

Table ES5. Cell 1, Free Space Loss, L_{FS} , and Measured Mean, 90%, and 99% L_{BT} Levels

D (km)	L_{FS}	L_{BT} (dB): 440 MHz			L_{FS}	L_{BT} (dB): 1360 MHz			L_{FS}	L_{BT} (dB): 1920 MHz		
		Mean	90%	99%		Mean	90%	99%		Mean	90%	99%
0.6	81.5	102.5	112.9	118.0	91.3	118.2	130.3	134.0	94.3	112.2	124.1	126.7
1.0	85.7	107.6	113.4	118.7	95.5	124.5	133.0	137.9	98.5	118.8	132.2	135.8
2.1	91.6	121.3	129.3	131.8	101.4	132.9	140.9	149.6	104.4	131.6	138.3	142.6
3.1	95.0	131.7	141.1	144.7	104.8	144.9	156.5	160.7	107.8	143.5	152.8	155.1
4.1	97.5	134.0	140.3	142.8	107.3	150.7	159.0	162.5	110.3	149.4	156.6	159.4
5.1	99.4	134.5	144.3	146.9	109.2	153.9	163.8	165.2	112.2	151.6	161.0	162.9
6.1	101.0	134.7	144.8	146.6	110.8	149.8	163.3	165.0	113.8	143.5	160.7	162.4
7.1	102.3	127.4	136.2	137.7	112.1	157.5	164.2	165.3	115.1	155.0	162.8	163.5
8.1	103.5	140.2	141.9	142.6	113.3	152.4	154.5	156.2	116.3	154.0	156.3	158.3

Table ES6. Cell 2, Free Space Loss, L_{FS} , and Measured Mean, 90%, and 99% L_{BT} Levels

D (km)	L_{FS}	L_{BT} (dB): 440 MHz			L_{FS}	L_{BT} (dB): 1360 MHz			L_{FS}	L_{BT} (dB): 1920 MHz		
		Mean	90%	99%		Mean	90%	99%		Mean	90%	99%
1.0	85.7	100.3	102.8	104.2	95.5	112.4	115.0	116.3	98.5	117.3	126.2	129.6
1.7	89.9	95.4	100.7	104.1	99.7	108.2	110.6	111.6	102.7	111.8	116.1	117.6
3.0	94.8	103.5	107.8	115.8	104.6	117.3	121.6	128.7	107.6	115.6	122.1	127.1
4.9	99.2	121.3	130.4	137.1	109.0	132.6	148.8	156.7	112.0	132.0	147.5	153.9
6.9	102.0	112.9	118.6	121.3	111.8	125.0	133.7	138.2	114.8	120.7	138.6	142.1
8.8	104.2	122.3	126.4	129.7	114.0	131.9	148.8	150.9	117.0	126.5	152.1	154.7
10.1	105.4	126.2	133.7	137.2	115.2	136.0	147.8	150.1	118.2	133.5	146.1	148.9
12.0	106.9	118.8	122.2	124.0	116.7	132.2	134.7	136.5	119.7	124.1	126.9	129.1
14.0	108.2	122.4	125.7	127.0	118.0	129.5	135.0	136.2	121.0	122.3	124.3	125.1
15.9	109.3	124.2	126.9	130.9	119.1	128.5	139.0	139.5	122.1	126.5	136.8	137.5
17.8	110.3	123.0	124.8	126.6	120.1	134.0	143.7	146.5	123.1	129.0	140.2	145.3
19.8	111.2	122.0	123.8	128.2	121.0	131.2	133.9	134.4	124.0	126.2	130.5	133.5
23.0	112.5	123.3	124.5	125.2	122.4	137.7	139.8	140.1	125.3	133.7	135.0	135.4
25.6	113.5	126.8	133.9	138.4	123.3	145.4	153.2	161.0	126.3	140.9	151.0	156.9

LIST OF FIGURES

	Page
Figure 2.1. Map showing Edwards Air Force Base and the transmitter locations.....	14
Figure 4.1. Basic transmission loss scatterplot, Cell 1, Route 1.....	15
Figure 4.2. Basic transmission loss scatterplot, Cell 1, Route 2.....	16
Figure 4.3. Basic transmission loss scatterplot, Cell 2, Route 1.....	17
Figure 4.4. Basic transmission loss scatterplot, Cell 2, Route 2.....	18
Figure 4.5. Basic transmission loss variance, Cell 1, 440 MHz.....	19
Figure 4.6. Basic transmission loss variance, Cell 1, 1360 MHz.....	19
Figure 4.7. Basic transmission loss variance, Cell 1, 1920 MHz.....	20
Figure 4.8. Basic transmission loss variance, Cell 2, 440 MHz.....	20
Figure 4.9. Basic transmission loss variance, Cell 2, 1360 MHz.....	21
Figure 4.10. Basic transmission loss variance, Cell 2, 1920 MHz.....	21
Figure 4.11. Basic transmission loss route map, Cell 1, Route 1, 440 MHz.....	22
Figure 4.12. Basic transmission loss route map, Cell 1, Route 1, 1360 MHz.....	22
Figure 4.13. Basic transmission loss route map, Cell 1, Route 1, 1920 MHz.....	23
Figure 4.14. Basic transmission loss route map, Cell 1, Route 2, 440 MHz.....	23
Figure 4.15. Basic transmission loss route map, Cell 1, Route 2, 1360 MHz.....	24
Figure 4.16. Basic transmission loss route map, Cell 1, Route 2, 1920 MHz.....	24
Figure 4.17. Basic transmission loss route map, Cell 2, Route 1-2, 440 MHz.....	25
Figure 4.18. Basic transmission loss route map, Cell 2, Route 1-2, 1360 MHz.....	25
Figure 4.19. Basic transmission loss route map, Cell 2, Route 1-2, 1920 MHz.....	26
Figure 5.1. Idealized impulse response diagram with descriptive terminology.....	27

	Page
Figure 5.2. Cell 1, Route 1, 20 dB ID: maximum delay CDF.....	28
Figure 5.3. Cell 1, Route 1, 20 dB ID: mean delay CDF.....	28
Figure 5.4. Cell 1, Route 1, 20 dB ID: RMS delay spread CDF.....	29
Figure 5.5. Cell 1, Route 2, 20 dB ID: maximum delay CDF.....	29
Figure 5.6. Cell 1, Route 2, 20 dB ID: mean delay CDF.....	30
Figure 5.7. Cell 1, Route 2, 20 dB ID: RMS delay spread CDF.....	30
Figure 5.8. Cell 2, Route 1, 20 dB ID: maximum delay CDF.....	31
Figure 5.9. Cell 2, Route 1, 20 dB ID: mean delay CDF.....	31
Figure 5.10. Cell 2, Route 1, 20 dB ID: RMS delay spread CDF.....	32
Figure 5.11. Cell 2, Route 2, 20 dB ID: maximum delay CDF.....	32
Figure 5.12. Cell 2, Route 2, 20 dB ID: mean delay CDF.....	33
Figure 5.13. Cell 2, Route 2, 20 dB ID: RMS delay spread CDF.....	33
Figure 5.14. Cell 1, Route 1, 10 dB ID: maximum delay CDF.....	34
Figure 5.15. Cell 1, Route 1, 10 dB ID: mean delay CDF.....	34
Figure 5.16. Cell 1, Route 1, 10 dB ID: RMS delay spread CDF.....	35
Figure 5.17. Cell 1, Route 2, 10 dB ID: maximum delay CDF.....	35
Figure 5.18. Cell 1, Route 2, 10 dB ID: mean delay CDF.....	36
Figure 5.19. Cell 1, Route 2, 10 dB ID: RMS delay spread CDF.....	36
Figure 5.20. Cell 2, Route 1, 10 dB ID: maximum delay CDF.....	37
Figure 5.21. Cell 2, Route 1, 10 dB ID: mean delay CDF.....	37
Figure 5.22. Cell 2, Route 1, 10 dB ID: RMS delay spread CDF.....	38
Figure 5.23. Cell 2, Route 2, 10 dB ID: maximum delay CDF.....	38

	Page
Figure 5.24. Cell 2, Route 2, 10 dB ID: mean delay CDF.....	39
Figure 5.25. Cell 2, Route 2, 10 dB ID: RMS delay spread CDF.....	39
Figure A1. Antenna patterns measured at Table Mountain showing gain above isotropic versus van azimuth.....	42
Figure A2. Gain of 440 MHz Cushcraft transmitter dipole (NIST Chamber).....	43
Figure A3. 1360 MHz Larson receiving monopole pattern (NIST Chamber).....	44
Figure A4. 1920 MHz Andrew receiving monopole (NIST Chamber).....	46

LIST OF TABLES

		Page
Table 1.	ATB Data Acquisition and RF Parameters.....	4
Table 2.	Overview of the Transmit and Receive Antenna Characteristics	5
Table 3.	Basic Transmission Loss, L_{BT} , Data for Cell 1 Route 1 (Low Transmitter, Short-Range Route).....	6
Table 4.	Basic Transmission Loss, L_{BT} , Data for Cell 1 Route 2 (Low Transmitter, Long-Range Route).....	7
Table 5.	Basic Transmission Loss, L_{BT} , Data for Cell 2 Route 1 (High Transmitter, Short-Range Route).....	7
Table 6.	Basic Transmission Loss, L_{BT} , Data for Cell 2 Route 2 (High Transmitter, Long-Range Route).....	8
Table 7.	Cell 1, Free Space Loss, L_{FS} , and Measured Mean, 90%, and 99% L_{BT} Levels.....	8
Table 8.	Cell 2, Free Space Loss, L_{FS} , and Measured Mean, 90%, and 99% L_{BT} Levels.....	9
Table 9.	Cell 1, Route 1 (Low Transmitter, Short-Range Route): Delay Statistics for APDP with a 20 dB ID.....	11
Table 10.	Cell 1, Route 2 (Low Transmitter, Long-Range Route): Delay Statistics for APDP with a 20 dB ID.....	11
Table 11.	Cell 2, Route 1 (High Transmitter, Short-Range Route): Delay Statistics for APDP with a 20 dB ID.....	11
Table 12.	Cell 2, Route 2 (High Transmitter, Long-Range Route): Delay Statistics for APDP with a 20 dB ID.....	11
Table 13.	Cell 1, Route 1 (Low Transmitter, Short-Range Route): Delay Statistics for APDP with a 10 dB ID.....	12
Table 14.	Cell 1, Route 2 (Low Transmitter, Long-Range Route): Delay Statistics for APDPS with a 10 dB ID.....	12

	Page
Table 15. Cell 2, Route 1 (High Transmitter, Short-Range Route): Delay Statistics for APDPS with a 10 dB ID.....	12
Table 16. Cell 2, Route 2 (High Transmitter, Long-Range Route): Delay Statistics for APDPS with a 10 dB ID.....	12
Table A1. Source Antenna Gain Data used for the Far Field Tests.....	41
Table A2. Gain Measurements for the Receiving Antennas.....	41
Table A3. Gain Measurements for the Transmitting Antennas.....	41
Table A4. 1360 MHz Dorne & Margolin Gain Measurements versus Azimuth Angle.....	42
Table A5. Averaged Table Mountain Azimuth Gain Measurements.....	43
Table A6. Gain Measured in the NIST Anechoic Chamber for the Receiving Monopole Antennas.....	45
Table A7. Receiving Antenna Gain.....	46
Table A8. Transmitting Antenna Gain.....	46
Table B1. EIRP Transmitted at EAFB.....	47
Table B2. Receiving Antenna Gains.....	47
Table B3. Transmitter Antenna Gains.....	47

This Page Intentionally Left Blank

This Page Intentionally Left Blank

**FLEXIBLE INTEROPERABLE TRANSCEIVER (FIT) PROGRAM
TEST RANGE I: RADIO PROPAGATION MEASUREMENTS AT 440, 1360 AND
1920 MHz EDWARDS AIR FORCE BASE, CA**

Peter Papazian, Perry Wilson, Michael Cotton and Yeh Lo*

Radiowave propagation measurements at Edwards Air Force Base, CA are described. These measurements were made as part of the Flexible Interoperable Transceiver (FIT) Program. The objective of the measurements is to define communication link requirements at 440, 1360, and 1920 MHz. Simultaneous wideband measurements at three frequencies were made using fixed transmitters and a mobile fitted with a multi-channel receiver. The system measured the radio channel impulse response. Data outputs include delay spread and basic transmission loss. These parameters are compared at the three measurement frequencies to determine additional propagation impairments military systems will suffer due to frequency translation from 440 MHz to 1360 MHz and 1920 MHz.

Key Words: impulse response; radiowave propagation; Flexible Interoperative Transceiver; FIT; delay spread; basic transmission loss.

1. INTRODUCTION

This report describes mobile communication link measurements made at Edwards Air Force Base, CA as part of the Flexible Interoperable Transceiver** (FIT) program. Edwards Air Force Base (EAFB) is the first of four locations to be measured, the other three being Fort Hood, TX, Fort Polk, LA and Camp Lejeune, NC. The goal of the measurement series is to define communication link characteristics at different frequencies over a representative cross section of military installations.

The primary figures of merit used here to characterize wireless communication links are basic transmission loss and delay statistics. Basic transmission loss is the signal attenuation between the transmitting and receiving antennas due to path length, shadowing, and scattering. Basic transmission loss determines the range of the link if the transmit power and receiver sensitivity are known. The delay statistics quantify the signal power received over the direct, or shortest path (first arriving signal), versus the later multipath signals. Delay statistics are important in determining bit error rates and equalizer design.

Three frequencies are considered: 440 MHz, 1360 MHz, and 1920 MHz. 440 MHz is representative of several current ground-to-ground communication links (JRTC-IS,

* The authors are with the Institute for Telecommunication Sciences, National Telecommunications and Information Administration, U.S. Department of Commerce, Boulder, CO 80303.

** This work was sponsored by U.S. Army STRICOM, 12350 Research Parkway, Orlando, FL 32826.

PRIME, PLRS). 1360 MHz is proposed for the next generation FIT system. 1920 MHz has similar characteristics to the 1710-1850 MHz band, which is also under consideration for FIT. By comparing the 1360 MHz and 1920 MHz basic transmission loss and delay statistics to those for 440 MHz, the viability of using higher frequencies for future military communications and the associated system requirements can be assessed.

The report is organized as follows. Section 2 gives a brief description of the measurement site. Two transmitter locations were used along with two drive routes yielding four cell-route combinations. Section 3 gives a brief overview of the ITS channel sounding system. The system uses a known pseudo-noise source that when received and processed closely approximates an ideal impulse signal over a wide bandwidth. Sections 4 and 5 detail the basic transmission loss measurements and delay statistics data. Section 6 gives the references and the figures are collected in Section 7 of the report.

2. SITE DESCRIPTION

EAFB is located in the desert approximately 160 km northwest of Los Angeles (see Figure 2.1). The primary functions of the base are to test experimental aircraft and to train test pilots. The predominant geographic feature of the site is a large dry lakebed. The lakebed is perfectly flat and an ideal runway surface. The lakebed is also ideal for transmission of radio signals, as there are no terrain features to obstruct radio wave propagation. The flight line is located on the west side of the main lakebed. This area has numerous 1 to 4 story buildings. They include large metal hangars with flat metal walls that are excellent reflectors of radio signals. Scattering and multipath impair radio propagation in this area. To the west of the flight line is the Werry Housing complex that resembles a suburban area with a few low-rolling hills. The rest of the base is generally desert terrain with scant vegetation, hills and some low mountains. The lakebed is at an elevation of about 693 m with hill and mountain elevations ranging from 701 to 915 m. The hills can obstruct radio signal propagation but are also good transmitter sites.

For this survey, two transmitter sites were chosen. Site 1 was located on the NW corner of the roof of building 3950 near the flight line. The ground elevation at this site was 701 m and the transmitter antennas were at a height of 706 m. This site was chosen to simulate a low, close-in transmitter, in the clutter of the flight-line buildings. Such a site might be used to communicate with aircraft on the flight-line and personnel and data terminals near the flight line buildings. It was expected that this site would have high path loss and multipath typical of a suburban cellular base station.

Site 2 was placed on the roof of the AF-38 radar on a prominent hill northeast of the flight line and site 1. Ground elevation at the site is 805 m and the transmitter antennas were at an elevation of 809 m. This site was chosen as representative of an optimum transmitter site for long range communication. It had a good view of the buildings near the flight line, the dry lakebed, the Werry housing complex and the base to the south, north and west. Towards the SE and the main entrance of the base, its view was obscured by Rosamond Hills, a 914 to 975 m high ridge line.

Two routes were chosen for use with both transmitter sites. Route 1 (e.g., see Figure 4.11) followed the base shuttle route. This route stayed within the built-up areas of the base. The range was generally short (< 7 km), and it was expected to have higher path loss and more multipath. Route 2 (e.g., see Figure 4.14) was selected as a long distance path (up to 25 km) traversing much of the base roads as well as the south base area. Route 1 was identical for both transmitter sites. Route 2 was similar for both transmitter sites except that a longer-range segment was added for transmitter site 2. This path extended NE to the town of Boron approximately 20 km away and provided a clear line of sight across the dry lakebed between transmitter site 2 and Boron. Route 2 was expected to have lower path loss and fewer multipath effects due to the high transmitter site and more rural nature of the areas traversed.

3. MEASUREMENT SYSTEM

The Institute for Telecommunication Sciences (ITS) ATB (antenna test bed) system used for these measurements is designed for measuring the radio channel impulse response. It can measure radio propagation parameters at multiple frequencies or from multiple antenna elements. It is also used for the comparative testing of diversity schemes, adaptive antenna systems, and data processing algorithms. The key elements of the acquisition system are: 1) up to 8 simultaneous channels, 2) broadband channel impulse sounding, 3) high speed analog to digital data conversion and storage, and 4) flexible post processing. The multi-channel sounder uses an upgraded version of the ITS digital channel probe (DCP). This probe has been used in previous programs (Motorola, USWEST, and PACTEL) to make impulse response measurements in the 900-MHz cellular and 1900-MHz PCS bands [1-3]. The system transmits a maximal-length pseudo noise (PN) code. The PN code is biphase shift key (BPSK) modulated onto an RF carrier. The transmitter is both frequency and bit-rate agile and can produce multiple PN codes and frequencies simultaneously. The transmitted signal, modified by the radio channel, is received, down-converted to an intermediate frequency (IF), and then digitized. If desired, the in-phase and quadrature-phase components can then be determined by post processing the data. The impulse response is generated by cross correlating a copy of the transmitted PN code with the received signal after it has been converted to base band. This step is usually done after the measurement, but it can also be done in real time using on board digital signal processors.

For the measurements reported here, the probe was configured to transmit a 511-bit PN word at 10 Mb/s on 440 MHz, 1360 MHz, and 1920 MHz carriers. The theoretical impulse signal to correlation noise ratio is 54 dB for a 511-bit PN sequence. The processing gain of the system is 27 dB. This means that when the signal power equals the noise power, the peak of the impulse response will be 27 dB above the noise. These parameters allow detection of multipath delays as great as 51 μ s and resolution of multiple delays spaced as closely as 100 ns. Since the system measures propagation time, the first arrival for signals traveling more than 16 km must be shifted in software so delayed signals will not wrap and appear to arrive first. This is easily done using the GPS

coordinates and adding time offsets to the data at large transmitter receiver separations. System timing is maintained using rubidium oscillators at the transmitter and receiver. These clocks synchronize the PN code generators, phase lock all local oscillators and provide sampling clocks for the digitizers. The oscillators' frequency stability ensures absolute timing measurements to within 50 ns for an 8-hour measurement period. It also allows measurement of the Doppler spectrum with 1 Hz accuracy. Data acquisition is controlled by multiple digital signal processors (DSPs) and a host computer system. Acquisition was set to the burst mode for these tests. In this mode, a burst of data is collected in rapid sequence and stamped with GPS coordinates and time. The next data burst is acquired after a programmable delay that was set to 10 seconds for these measurements. Within a burst, the delay between impulses (51 μ s in length) was set to 3 ms. The number of impulses per burst was set to 128, resulting in an overall burst duration of approximately 388 ms. Table 1 summarizes the data acquisition parameters used for the diversity measurements, as well as the range of permissible values for the ATB system. Block diagrams for the system can be found in [4].

Mobile receiving antennas (RX) and fixed transmitting antennas (TX) were used. The transmitting antennas were mounted on tripods at locations described in Section 2. The mobile receivers used omni-directional "whip" antennas. Receiving antennas were mounted at a height of 2.4 m on a van equipped with a GPS/dead reckoning system. The receive antenna patterns and gains were measured in situ on the van and in an anechoic chamber using a 1.3 m diameter ground plane. An overview of the antenna characteristics is given in Table 2 (H = horizontal, V = vertical).

Vertical plane antenna gains were measured over ground using a clear line of sight. The measured data agree with manufacturer's specifications only for the 1360- and 1920-MHz transmit antennas. Differences arise due to cables, connectors and environment. One important effect is the van roof that only approximates an infinite ground screen. This causes the vertical directivity of the receive antennas to peak near 20° [5]. Thus at an elevation angle of 0° these antennas can have gains less than an isotropic radiator, as is the case for the 1360- and 1920-MHz antennas (-1.3 and -0.7 dB respectively). For more detail on antenna calibrations see Appendix A.

Table 1. ATB Data Acquisition and RF Parameters

Configurable System Parameters		
Parameter	Present Diversity Tests	ATB System
Receiver Channels	3	1-8
Carrier Frequencies	440, 1360, 1920 MHz	.45 – 6 GHz
Bit Rate	10 Mb/s	.1 – 50 Mb/s
Resolution	100 ns	10 μ s – 20 ns
Code Type	Maximal Length	Programmable
Code Length	511 bits	Programmable
Acquisition Mode	Burst	Continuous or Burst
Positioning	GPS/Dead Reckoning	GPS/Dead Reckoning
Transmitters	3	Multiple
Data Processing	Post	Post or Real Time

Table 2. Overview of the Transmit and Receive Antenna Characteristics

	440 MHz	1360 MHz	1920 MHz
Frequency	440 MHz	1360 MHz	1920 MHz
TX Antennas			
Type	Cushcraft FRX-430 Dipole	Dorne and Margolin DM Q130 Dipole	Andrew PC1N0F-019A-006 Dipole
H-Plane Pattern	Omni-directional	Directional *	Omni-directional
V-Plane Gain (dBi)	1.7	11.3	6.9
RX Antennas			
Type	Larson $5/8\lambda$ monopole	Larson Base with $1/4\lambda$ monopole	Andrew magmount PCS monopole
H-Plane Pattern	Omni-directional	Omni-directional	Omni-directional
V-Plane Gain (dBi)	1.2	-1.3	-0.7

* 160 degree 3 dB beamwidth, azimuth pattern from lookup table.

4. BASIC TRANSMISSION LOSS

Basic transmission loss (L_{BT}), is the signal attenuation between transmit and receive antennas due to free space, or spreading loss (L_{FS}), and signal attenuation. Basic transmission loss determines the range of the link. Basic transmission loss is given by

$$L_{BT}(dB) = P_t(dB) - P_r(dB) + G_t(dB) + G_r(dB) \quad (4.1)$$

where P_t is the transmitted power, P_r is the received power, G_t is the transmit antenna gain, and G_r is the receive antenna gain. An ideal free space (FS) path (no ground reflection, no multipath, no signal attenuation) has a path loss which is proportional to the square ($n = 2$) of the separation D

$$L_{FS}(d) = 10n \log_{10} \left(\frac{4\pi D}{\lambda} \right)_{n=2} \quad (4.2)$$

where λ is the wavelength. This typically represents the minimum path loss and serves as a lower limit. Values of n on the order of 4 are more representative of the cluttered environments and low transmit antenna heights found at cellular base stations in built-up areas.

4.1 Path Loss Data and Discussion

The basic transmission loss (L_{BT}) versus distance is plotted in Figures 4.1 through 4.4 for three frequencies (440 MHz, 1360 MHz, and 1920 MHz). Each point in these scatter plots represents an average over a burst (128 impulses, all impulses within a burst have

the same GPS location tag). The figures show the four cell-route combinations. The data are then fit with a curve of the form

$$\overline{L_{BT}} = n \times 10 \log_{10}(BD), \quad (4.3)$$

where $n = \text{path loss exponent}$
 $D = \text{distance (km)}$
 $B = \text{distance multiplier}.$

This curve is linear with a slope of n when plotted on a log-log scale. Free space path loss (L_{FS}) is also plotted for the same three frequencies. The free-space curves serve as a “minimum” loss reference.

One loss parameter of interest is the ratio of the measured loss to the free space loss at a given frequency, designated $\Delta L_{BT/FS}$. This parameter gives an indication of the additional loss due to scattering and diffraction within the channel. Also of interest is the ratio of the measured loss at 1360 MHz and 1920 MHz to the measured loss at 440 MHz, designated $\Delta L_{BT/440}$. This parameter gives an indication of the additional power needed at these higher frequencies when compared to the existing 440 MHz systems. These two parameters will be highlighted in the discussion that follows and in Tables 3 to 6.

Figure 4.1 shows the L_{BT} data measured in Cell 1 (low transmitter site) along Route 1. This route includes multipath and shadowing caused by buildings near the flight line. From the curve fit data we see that the path loss exponent n , for the 440 MHz and 1920 MHz data is about 4, while n for 1360 is about 3.1. These values are about twice that of free space ($n = 2$). L_{BT} is larger than for free space at all distances and this difference increases as distance increases. For example, at 0.7 km, the 440 MHz, 1360 MHz and 1920 MHz $L_{BT/FS}$ values are 24.2 dB, 26.0 dB and 21.9 dB respectively. The loss ratio at the two higher frequencies ($\Delta L_{BT/440}$) at 0.7 km is approximately 11.6 dB (1360 MHz) and 10.5 dB (1920 MHz). Because the 1360 MHz curve fit slope is smaller than the 440 MHz curve fit slope, $\Delta L_{BT/440}$ for 1360 MHz becomes smaller at greater distances while $\Delta L_{BT/440}$ for 1920 MHz remains almost constant. These data are summarized in Table 3.

Table 3. Basic Transmission Loss, L_{BT} , Data for Cell 1, Route 1 (Low Transmitter, Short-Range Route)

F (MHz)	L_{BT} Linear Fit Parameters		D 0.7 km		
	n	B (km^{-1})	L_{FS} (dB)	$\Delta L_{BT/FS}$ (dB)	$\Delta L_{BT/440}$ (dB)
440	3.8	9.0e+2	82.2	24.2	0.0
1360	3.1	9.1e+3	92.0	26.0	11.6
1920	4.1	1.0e+3	95.0	21.9	10.5

The data from Cell 1, Route 2 (long-range route) exhibited a different set of path loss exponents. At 440 MHz, the path loss exponent dropped to a near free space value of 1.9. The 1360 MHz path loss exponent is 4.6 and the 1920-MHz exponent is 3.9. It appears that the low n at 440 MHz is due to the relatively small L_{BT} values at distances between 5 and 8 km that decreased the overall slope of the curve fit. $\Delta L_{BT/FS}$ at 440 MHz varies only slightly from 31.9 dB to 31.5 dB, as the distance is increased from 3.0 to 8.0 km. $\Delta L_{BT/FS}$ at 1360 MHz ranges from 27.2 dB at 3km to 38.3 dB at 8 km. The equivalent 1920-MHz $\Delta L_{BT/FS}$ data are 29.8 dB to 37.8 dB. The higher frequency loss ratio $\Delta L_{BT/440}$ at 3.0 km and 8.0 km is 5.1 and 16.6 dB for 1360 MHz, and 10.7 dB and 19.2 dB for 1920 MHz. These values can be linearly interpolated for other distances in the measured range by multiplying the ratio of the distances in kilometers by the slope. These data are summarized in Table 4.

Data collected from the high transmitter site (Cell 2) are shown in Figures 4.3 and 4.4. For Cell 2, Route 1, all frequencies have path loss exponents (0.7 to 1.0) smaller than the free space value. We believe this is due to relatively constant shadowing of the transmitter by terrain and clutter on Route 1, and to the small variations in path length from the transmitter site. These factors result in an almost distance-independent path loss over this short range. The various loss parameters for Cell 2, Route 1 are summarized in Table 5.

Table 4. Basic Transmission Loss, L_{BT} , Data for Cell 1 Route 2 (Low Transmitter, Long-Range Route)

F (MHz)	L_{BT} Linear Fit Parameters		D					
			3.0 km			8.0 km		
			L_{FS} (dB)	$\Delta L_{BT/FS}$ (dB)	$\Delta L_{BT/440}$ (dB)	L_{FS} (dB)	$\Delta L_{BT/FS}$ (dB)	$\Delta L_{BT/440}$ (dB)
440	1.9	1.6e+6	94.9	31.9	0.0	103.4	31.5	0.0
1360	4.6	2.5e+2	104.7	27.2	5.1	113.2	38.3	16.6
1920	3.9	1.1e+3	104.7	29.8	10.7	116.2	37.8	19.2

Table 5. Basic Transmission Loss, L_{BT} , Data for Cell 2 Route 1 (High Transmitter, Short-Range Route)

F (MHz)	L_{BT} Linear Fit Parameters		D					
			4.5 km			6.5 km		
			L_{FS} (dB)	$\Delta L_{BT/FS}$ (dB)	$\Delta L_{BT/440}$ (dB)	L_{FS} (dB)	$\Delta L_{BT/FS}$ (dB)	$\Delta L_{BT/440}$ (dB)
440	0.7	3.3e+15	98.4	14.9	0.0	101.6	12.8	0.0
1360	0.9	4.8e+13	108.2	20.8	15.7	111.4	19.0	16.1
1920	1.0	4.5e+12	111.2	21.8	19.8	114.4	20.2	20.2

Data from Cell 2, Route 2 are shown in Figure 4.4. Here the slopes are all near 2 and run almost parallel to the free space curves. This route was dominated by line of sight

conditions across the dry lakebed to the NE of the high transmitter site. $\Delta L_{BT/FS}$ tabulated at distances of 2.0 and 20.0 km shows only small variations due to the nearly parallel slopes. These loss data for Cell 2, Route 2 are summarized in Table 6.

Table 6. L_{BT} , Data for Cell 2 Route 2 (High Transmitter, Long-Range Route)

F (MHz)	L_{BT} Linear Fit Parameters		D					
			2.0 km			20.0 km		
	n	B (km^{-1})	L_{FS} (dB)	$\Delta L_{BT/FS}$ (dB)	$\Delta L_{BT/440}$ (dB)	L_{FS} (dB)	$\Delta L_{BT/FS}$ (dB)	$\Delta L_{BT/440}$ (dB)
440	2.1	4.5e+4	91.3	12.8	0.0	111.3	13.8	0.0
1360	1.9	1.1e+6	101.1	19.1	16.2	121.1	18.1	14.2
1920	1.7	2.8e+6	104.1	10.7	10.7	124.1	7.7	6.7

An alternative to curve fitting the measured data is to bin the L_{BT} data according to distance and compute the mean, standard deviation, and the 90% and 99% probability levels (i.e., 99% of the L_{BT} data in the bin are less than this level). These data are plotted in Figures 4.5 to 4.10 and summarized in Tables 7 and 8. Note that in these plots the data are not averaged over a burst as in Figures 4.1 to 4.4. The 99% L_{BT} levels range from 126 to 163 (dB) in Cell 1 and from 117 to 157 dB in Cell 2. These data give the upper bounds for the measured transmission loss L_{BT} and indicate the transmit power level needed to ensure a certain channel availability probability.

The L_{BT} data also can be plotted on site maps as shown in Figures 4.11 to 4.22. These maps show the spatial distribution of L_{BT} along the various cell-route combinations.

Table 7. Cell 1, Free Space Loss, L_{FS} , and Measured Mean, 90%, and 99% L_{BT} Levels

D (km)	L_{FS}	L_{BT} (dB): 440 MHz			L_{FS}	L_{BT} (dB): 1360 MHz			L_{FS}	L_{BT} (dB): 1920 MHz		
		Mean	90%	99%		Mean	90%	99%		Mean	90%	99%
0.6	81.5	102.5	112.9	118.0	91.3	118.2	130.3	134.0	94.3	112.2	124.1	126.7
1.0	85.7	107.6	113.4	118.7	95.5	124.5	133.0	137.9	98.5	118.8	132.2	135.8
2.1	91.6	121.3	129.3	131.8	101.4	132.9	140.9	149.6	104.4	131.6	138.3	142.6
3.1	95.0	131.7	141.1	144.7	104.8	144.9	156.5	160.7	107.8	143.5	152.8	155.1
4.1	97.5	134.0	140.3	142.8	107.3	150.7	159.0	162.5	110.3	149.4	156.6	159.4
5.1	99.4	134.5	144.3	146.9	109.2	153.9	163.8	165.2	112.2	151.6	161.0	162.9
6.1	101.0	134.7	144.8	146.6	110.8	149.8	163.3	165.0	113.8	143.5	160.7	162.4
7.1	102.3	127.4	136.2	137.7	112.1	157.5	164.2	165.3	115.1	155.0	162.8	163.5
8.1	103.5	140.2	141.9	142.6	113.3	152.4	154.5	156.2	116.3	154.0	156.3	158.3

Table 8. Cell 2, Free Space Loss, L_{FS} , and Measured Mean, 90%, and 99% L_{BT} Levels

D (km)	L_{FS}	L_{BT} (dB): 440 MHz			L_{FS}	L_{BT} (dB): 1360 MHz			L_{FS}	L_{BT} (dB): 1920 MHz		
		Mean	90%	99%		Mean	90%	99%		Mean	90%	99%
1.0	85.7	100.3	102.8	104.2	95.5	112.4	115.0	116.3	98.5	117.3	126.2	129.6
1.7	89.9	95.4	100.7	104.1	99.7	108.2	110.6	111.6	102.7	111.8	116.1	117.6
3.0	94.8	103.5	107.8	115.8	104.6	117.3	121.6	128.7	107.6	115.6	122.1	127.1
4.9	99.2	121.3	130.4	137.1	109.0	132.6	148.8	156.7	112.0	132.0	147.5	153.9
6.9	102.0	112.9	118.6	121.3	111.8	125.0	133.7	138.2	114.8	120.7	138.6	142.1
8.8	104.2	122.3	126.4	129.7	114.0	131.9	148.8	150.9	117.0	126.5	152.1	154.7
10.1	105.4	126.2	133.7	137.2	115.2	136.0	147.8	150.1	118.2	133.5	146.1	148.9
12.0	106.9	118.8	122.2	124.0	116.7	132.2	134.7	136.5	119.7	124.1	126.9	129.1
14.0	108.2	122.4	125.7	127.0	118.0	129.5	135.0	136.2	121.0	122.3	124.3	125.1
15.9	109.3	124.2	126.9	130.9	119.1	128.5	139.0	139.5	122.1	126.5	136.8	137.5
17.8	110.3	123.0	124.8	126.6	120.1	134.0	143.7	146.5	123.1	129.0	140.2	145.3
19.8	111.2	122.0	123.8	128.2	121.0	131.2	133.9	134.4	124.0	126.2	130.5	133.5
23.0	112.5	123.3	124.5	125.2	122.4	137.7	139.8	140.1	125.3	133.7	135.0	135.4
25.6	113.5	126.8	133.9	138.4	123.3	145.4	153.2	161.0	126.3	140.9	151.0	156.9

5. DELAY STATISTICS

The delay statistics presented in this report are based on averaged power delay profiles (APDPs)

$$APDP(t_i) = \frac{1}{N} \sum_{k=1}^N PDP_k(t_i) \quad , \quad (5.1)$$

where t_i is the i -th time step (sampling point), and N is the number of PDPs used to form the APDP. The PDP is the magnitude squared (power) of the measured impulse response. The use of averaging significantly reduces the contribution of noise to the delay statistics. The ATB burst configuration software was set to produce a total of 128 impulses per burst for these measurements. APDPs are calculated from groups of 8 successive PDPs. Thus, each burst yields 16 APDPs (128/8). The choice of 8 as the group size makes efficient use of all the burst data. APDPs are computed separately for each channel.

Impulses within an APDP group (8 successive PDPs) were first checked for sufficient power. The impulse with the maximum total signal power was found by integration over the full time interval. Impulses with total signal power more than 10 dB below this group maximum were discarded for the APDP statistics. Groups containing less than 4 usable PDPs are discarded as well. Thus, N ranges from 4 to 8 in (5.1) above.

Referring to Figure 5.1, the interval of discrimination (ID) is here defined as the difference in power levels between the peak of the intended signal (impulse) and the peak noise. It is desired that an APDP have an ID sufficient to ensure that noise does not contaminate the fading statistics. For the data here, 23 dB and 13 dB ID criteria will be used. The 23-dB margin gives the maximum useful dynamic range for analog

applications, while the 13-dB threshold may be more useful for digital applications. If the ID was less than 23 dB or 13 dB respectively, then the APDP was discarded for that data set. For valid APDPs, signal levels within 20 dB and 10 dB respectively of the APDP peak are included in the delay statistics, as indicated in Figure 5.1. This corrected APDP ensures that noise is not included. We expect the 20 dB criterion to yield longer delays but fewer valid APDPs than will the 10 dB criterion.

Three delay measures were considered: maximum delay, mean delay, and RMS delay spread. The maximum delay was here defined as the time delay between the first and last signals of that portion of the corrected APDP (see Fig. 5.1). The mean delay (d) was the time-weighted average, or first moment, of the corrected APDPs normalized by the average signal power,

$$\text{mean delay} = d = \frac{\frac{1}{N} \sum_{k=1}^N t_k P(t_k)}{\frac{1}{N} \sum_{k=1}^N P(t_k)} = \frac{\sum_{k=1}^N t_k P(t_k)}{\sum_{k=1}^N P(t_k)}, \quad (5.2)$$

where t_k is the time delay (in seconds) relative to the start of the corrected APDP (i.e. $t = 0$), P is the signal power (W), and N is the index of the final corrected APDP signal point considered. The RMS delay spread (S) measures the standard deviation of the delay spread of each corrected APDP about its mean delay (d). It is the second central moment of the corrected APDP given by

$$\text{RMS delay spread} = S = \left[\frac{\sum_{k=1}^N (t_k - d)^2 P(t_k)}{\sum_{k=1}^N P(t_k)} \right]^{1/2}. \quad (5.3)$$

Figures 5.2 through 5.13 show the cumulative probability distributions (CDFs) for the four cell and route combinations using 23-dB ID and 20-dB corrected APDP levels. Figures 5.14 through 5.25 show the corresponding data for the 13 dB ID and 10 dB corrected APDP levels. The CDF data are summarized in Tables 9 through 16 which give the maximum delay (max), mean delay (avg), and RMS delay spread (spread) in microseconds observed at the 90%, 99%, and 99.9% confidence levels. Also included in the tables are the percentages of valid APDPs for each of the cell, route, and frequency combinations.

Table 9. Cell 1, Route 1 (Low Transmitter, Short-Range Route): Delay Statistics for APDP with a 20 dB ID

	440 MHz			1360 MHz			1920 MHz		
	49 % Valid Impulses			54 % Valid Impulses			64 % Valid Impulses		
Prob. (%)	Delay (μ s)			Delay (μ s)			Delay (μ s)		
	max	avg	spread	max	avg	spread	max	avg	spread
90.0	6.8	1.2	1.4	9.5	2.5	2.1	9.7	2.7	2.4
99.0	11.2	4.3	2.8	16.9	7.2	3.9	17.7	6.9	3.4
99.9	29.1	7.6	3.1	21.9	8.6	4.5	19.6	7.6	4.1

Table 10. Cell 1, Route 2 (Low Transmitter, Long-Range Route): Delay Statistics for APDPs with a 20 dB ID

	440 MHz			1360 MHz			1920 MHz		
	20 % Valid Impulses			42 % Valid Impulses			43 % Valid Impulses		
Prob. (%)	Delay (μ s)			Delay (μ s)			Delay (μ s)		
	max	avg	spread	max	avg	spread	max	avg	spread
90.0	8.7	1.9	2.0	10.1	1.5	2.2	19.0	2.4	3.9
99.0	20.8	9.3	5.5	19.4	6.5	4.2	24.9	9.2	8.9
99.9	25.6	10.2	8.3	24.8	7.7	4.9	28.8	11.4	9.2

Table 11. Cell 2, Route 1 (High Transmitter, Short Range Route): Delay Statistics for APDPs with a 20 dB ID

	440 MHz			1360 MHz			1920 MHz		
	70 % Valid Impulses			88 % Valid Impulses			87 % Valid Impulses		
Prob. (%)	Delay (μ s)			Delay (μ s)			Delay (μ s)		
	max	avg	spread	max	avg	spread	max	avg	spread
90.0	7.3	1.2	2.0	10.8	3.4	3.4	11.4	3.0	3.4
99.0	16.9	5.5	6.6	20.1	8.2	5.9	25.0	6.7	6.9
99.9	16.9	9.4	7.1	25.4	10.6	6.5	26.0	10.4	8.4

Table 12. Cell 2, Route 2 (High Transmitter, Long-Range Route): Delay Statistics for APDPs with a 20 dB ID

	440 MHz			1360 MHz			1920 MHz		
	61 % Valid Impulses			85 % Valid Impulses			83 % Valid Impulses		
Prob. (%)	Delay (μ s)			Delay (μ s)			Delay (μ s)		
	max	avg	spread	max	avg	spread	max	avg	spread
90.0	5.6	0.4	1.0	5.8	0.5	1.4	7.7	0.8	1.9
99.0	28.4	16.9	9.2	21.6	6.2	6.0	26.2	6.1	7.3
99.9	44.5	20.6	11.2	25.9	20.7	8.2	44.4	20.2	8.7

Table 13. Cell 1, Route 1 (Low Transmitter, Short-Range Route): Delay Statistics for APDPs with a 10 dB ID

	440 MHz			1360 MHz			1920 MHz		
	71 % Valid Impulses			77 % Valid Impulses			80 % Valid Impulses		
Prob. (%)	Delay (μ s)			Delay (μ s)			Delay (μ s)		
	max	avg	spread	max	avg	spread	max	avg	spread
90.0	3.7	1.3	1.4	2.4	1.7	1.7	7.6	2.7	2.1
99.0	8.9	4.2	3.2	6.0	3.6	3.6	16.0	6.4	4.0
99.9	15.3	5.9	4.6	7.4	7.4	4.3	20.2	8.3	6.4

Table 14. Cell 1, Route 2 (Low Transmitter, Long-Range Route): Delay Statistics for APDPs with a 10 dB ID

	440 MHz			1360 MHz			1920 MHz		
	52 % Valid Impulses			73 % Valid Impulses			75 % Valid Impulses		
Prob. (%)	Delay (μ s)			Delay (μ s)			Delay (μ s)		
	max	avg	spread	max	avg	spread	max	avg	spread
90.0	3.0	1.8	1.3	4.4	1.6	1.4	6.4	2.5	2.2
99.0	5.6	3.2	1.9	11.5	6.5	4.0	21.9	8.2	8.2
99.9	19.2	10.4	5.6	19.9	7.5	6.1	22.7	9.2	9.2

Table 15. Cell 2, Route 1 (High Transmitter, Short-Range Route): Delay Statistics for APDPs with a 10 dB ID

	440 MHz			1360 MHz			1920 MHz		
	96 % Valid Impulses			100 % Valid Impulses			100 % Valid Impulses		
Prob. (%)	Delay (μ s)			Delay (μ s)			Delay (μ s)		
	max	avg	spread	max	avg	spread	max	avg	spread
90.0	5.2	1.9	2.2	8.1	3.5	3.3	10.5	3.5	4.1
99.0	15.4	6.3	6.8	15.3	8.5	6.3	24.2	10.5	8.5
99.9	15.4	9.4	7.1	16.8	10.7	6.8	25.9	12.3	9.8

Table 16. Cell 2, Route 2 (High Transmitter, Long-Range Route): Delay Statistics for APDPs with a 10 dB ID

	440 MHz			1360 MHz			1920 MHz		
	85 % Valid Impulses			94 % Valid Impulses			94 % Valid Impulses		
Prob. (%)	Delay (μ s)			Delay (μ s)			Delay (μ s)		
	max	avg	spread	max	avg	spread	max	avg	spread
90.0	0.2	0.1	> 0.1	0.4	0.1	0.1	0.5	0.2	0.1
99.0	18.1	6.6	6.4	16.6	5.9	6.0	21.6	6.0	6.8
99.9	26.6	13.9	8.3	20.5	14.8	7.8	22.9	12.1	8.6

6. REFERENCES

- [1] J. A. Wepman, J. R. Hoffman, L. Loew and V. S. Lawrence, "Comparison of wideband propagation in the 902-928 and 1850-1990 MHz bands in various macrocellular environments," NTIA Report 93-299, Sep. 1993.
- [2] J. A. Wepman, J. R. Hoffman and L. Loew, "Impulse response measurements in the 1850-1990 MHz band in large outdoor cells," NTIA Report 94-309, June 1994.
- [3] P. Wilson, P. Papazian, M. Cotton and Y. Lo, "Advanced antenna test bed characterization for wideband wireless communication systems," NTIA Report 99-369, August 1999.
- [4] P. B. Papazian, K. Allen and M. Cotton, "A test bed for the evaluation of adaptive antennas used for mobile communications," in *Proc. IEEE Aerospace Conference*, Snowmass, CO, Mar. 1998, paper #161.
- [5] M. Weiner, S. Cruze, C. Li and W. Wilson, Ch. 3 of *Monopole Elements on Circular Ground Planes*, Norwood, MA: Artech House, 1987, pp. 19 - 76.

7. FIGURES

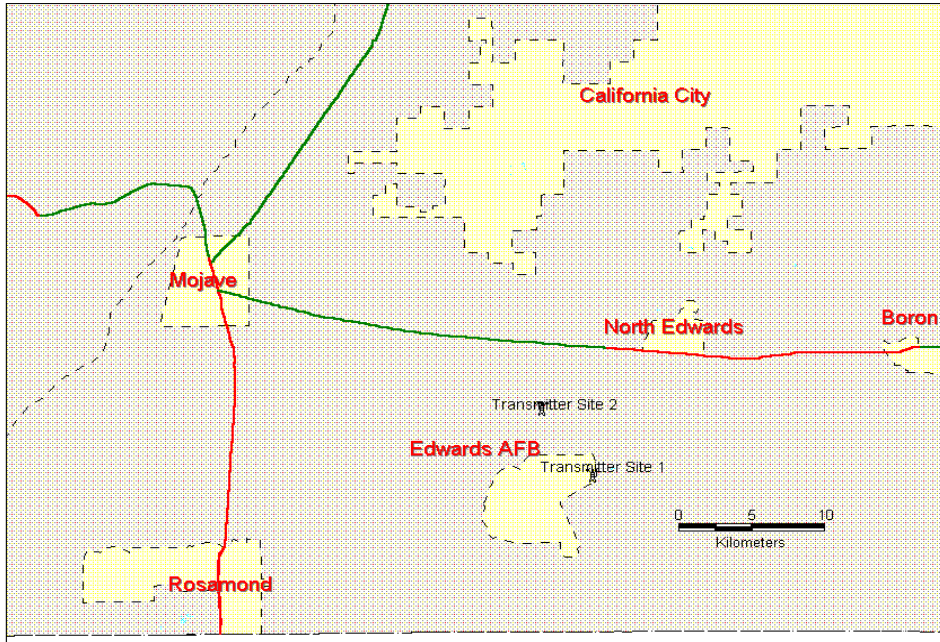


Figure 2.1. Map showing Edwards Air Force Base and the transmitter locations.

Edwards Air Force Base Cell 1, Route 1

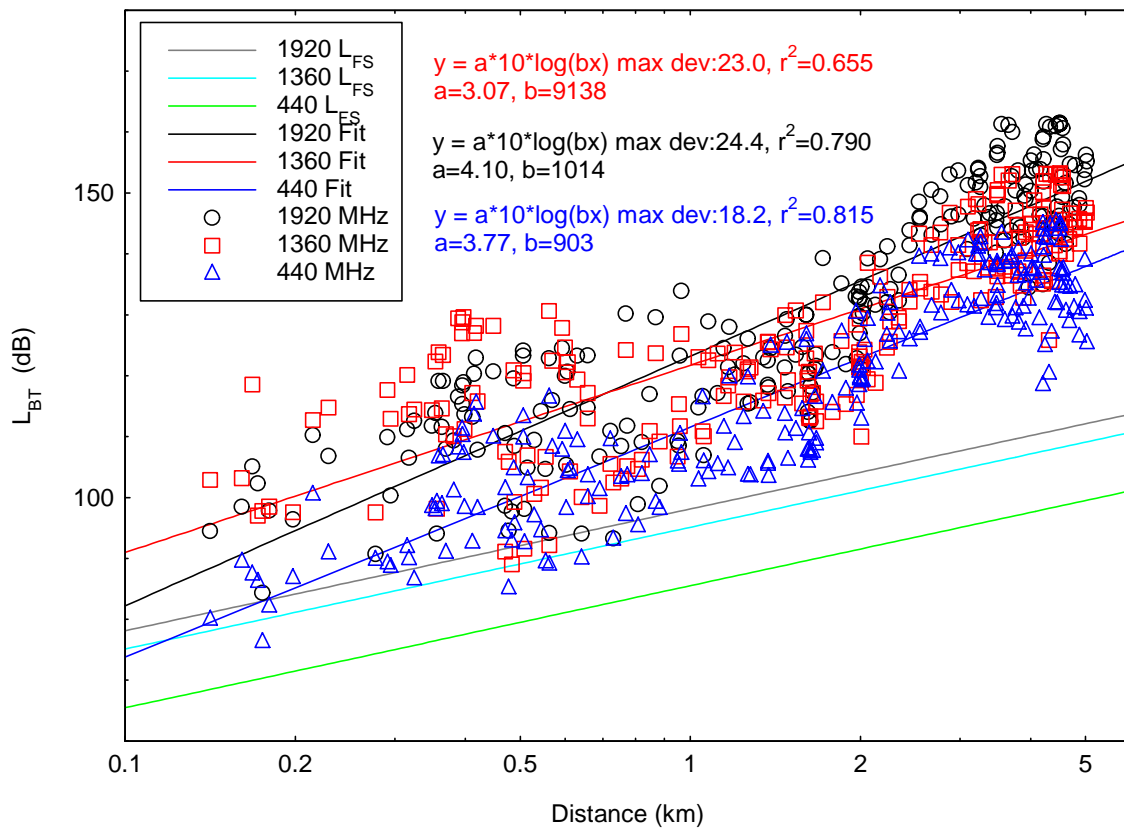


Figure 4.1. Basic transmission loss scatterplot, Cell 1, Route 1.

Edwards Air Force Base Cell 1, Route 2

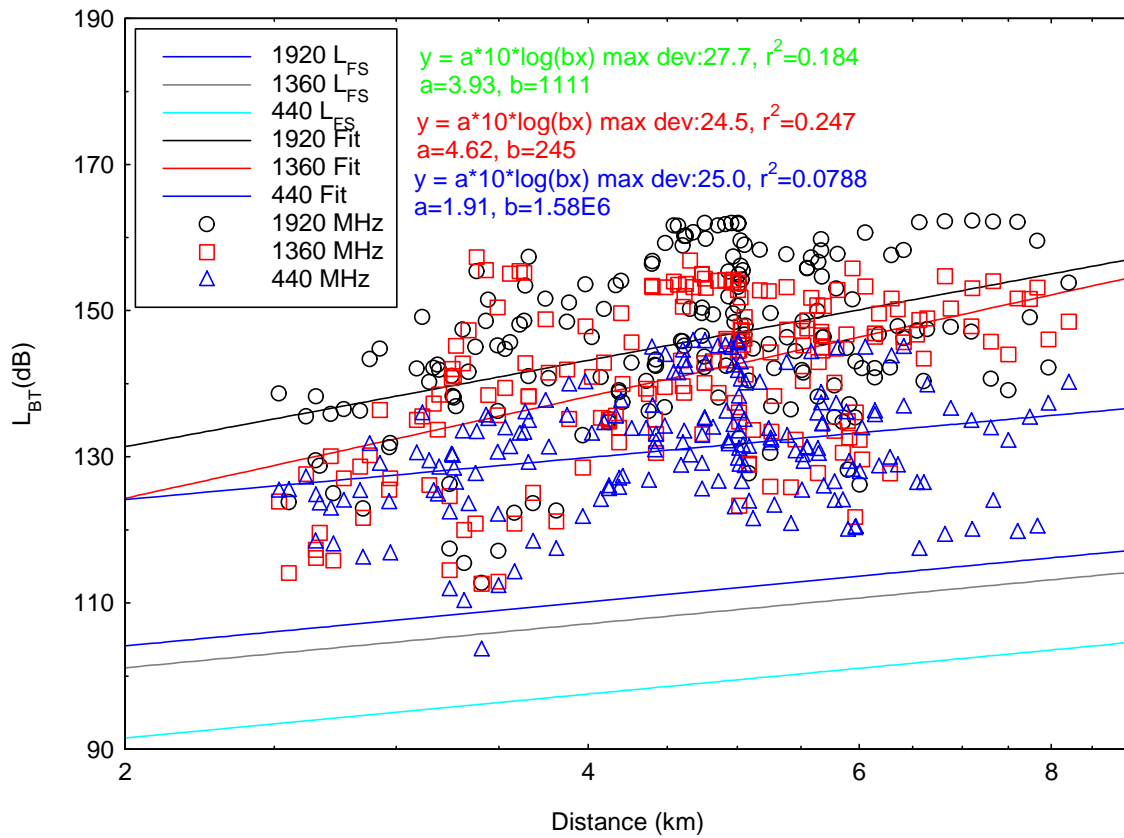


Figure 4.2. Basic transmission loss scatterplot, Cell 1, Route 2.

Edwards Air Force Base Cell 2, Route 1

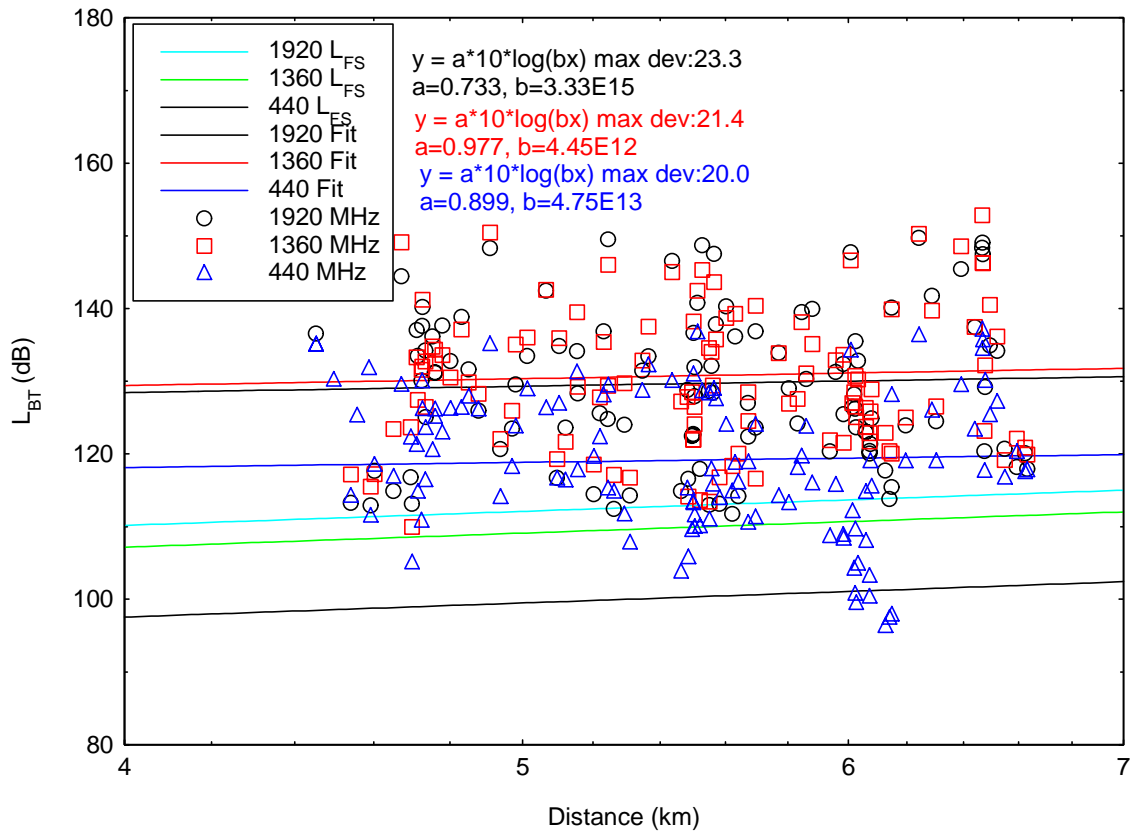


Figure 4.3. Basic transmission loss scatterplot, Cell 2, Route 1.

Edwards Air Force Base Cell 2, Route 2

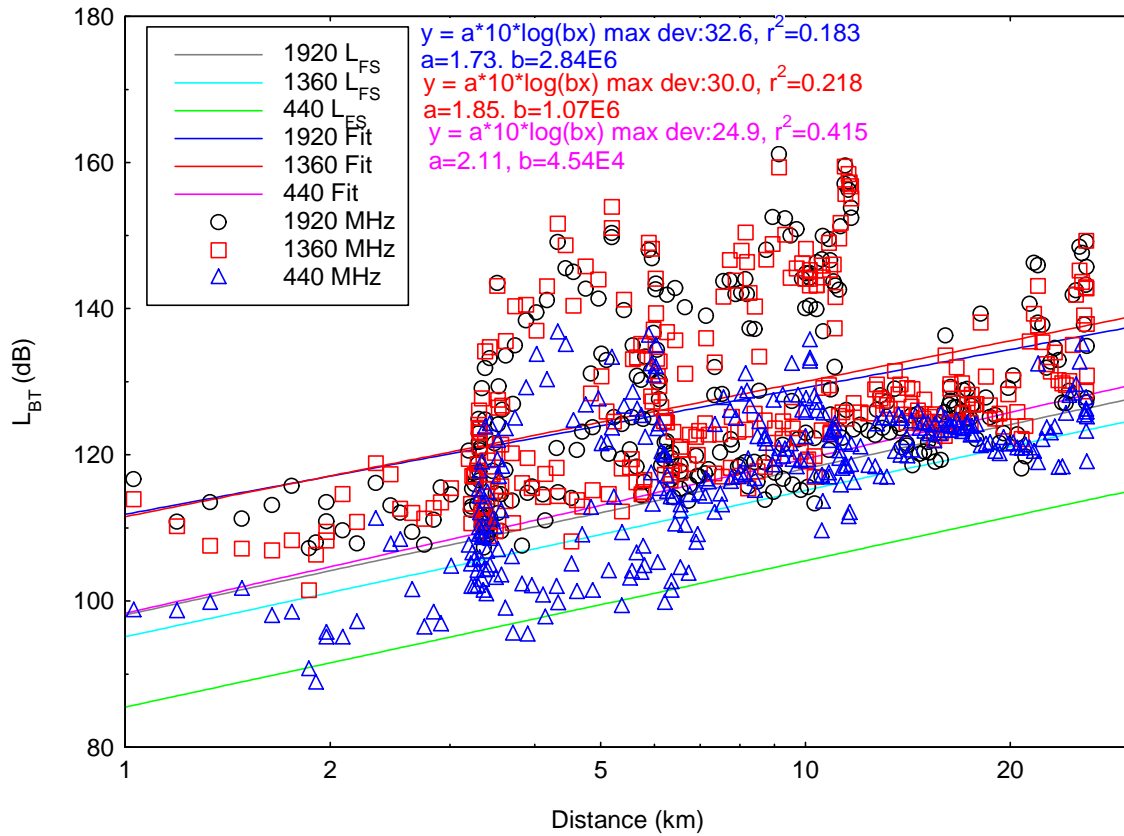


Figure 4.4. Basic transmission loss scatterplot, Cell 2, Route 2.

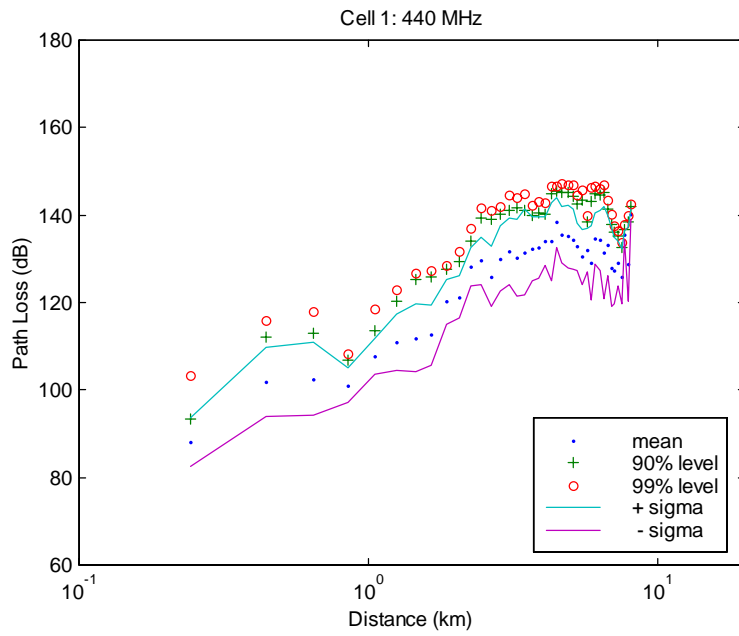


Figure 4.5. Basic transmission loss variance, Cell 1, 440 MHz.

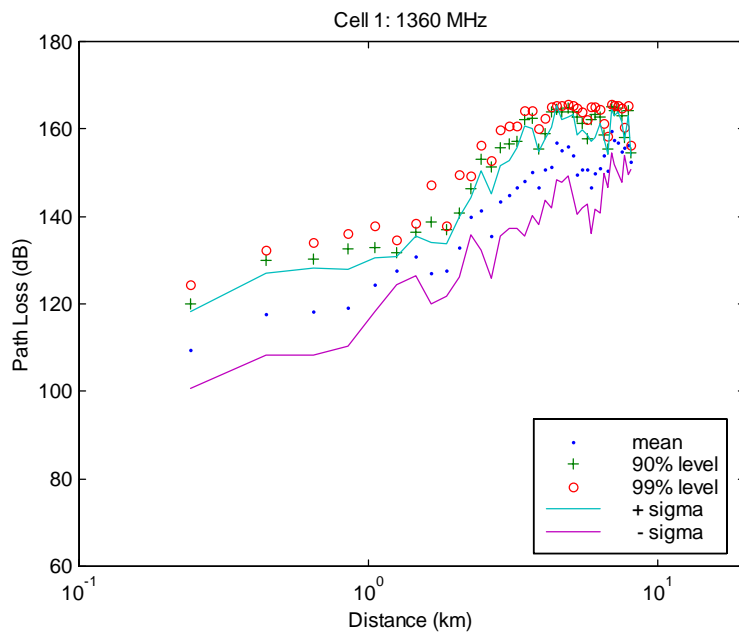


Figure 4.6. Basic transmission loss variance, Cell 1, 1360 MHz.

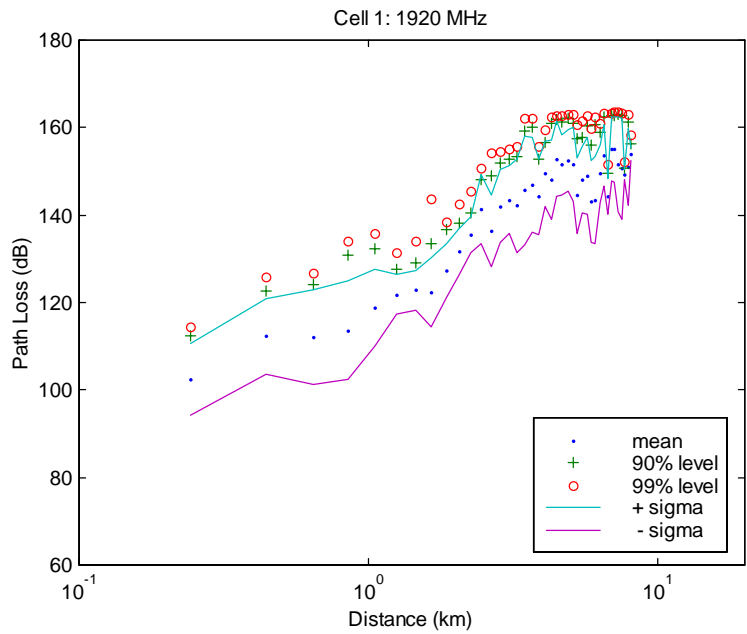


Figure 4.7. Basic transmission loss variance, Cell 1, 1920 MHz.

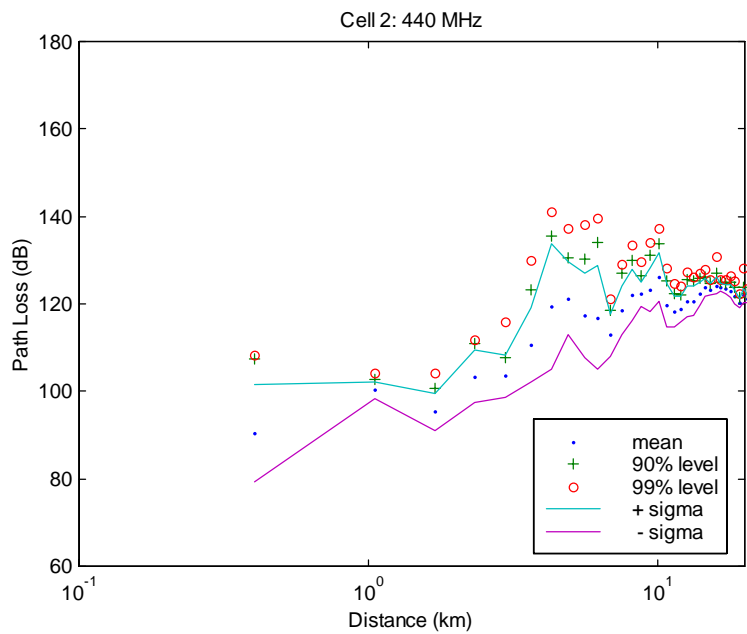


Figure 4.8. Basic transmission loss variance, Cell 2, 440 MHz.

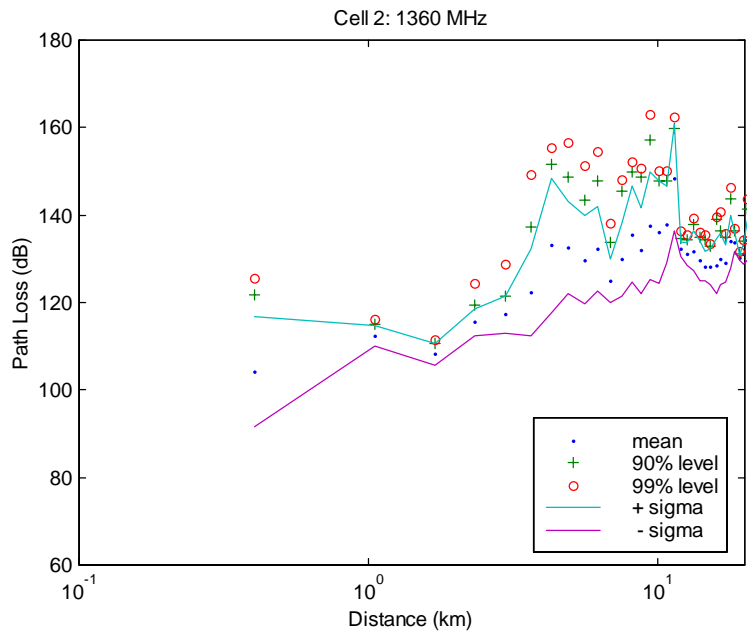


Figure 4.9. Basic transmission loss variance, Cell 2, 1360 MHz.

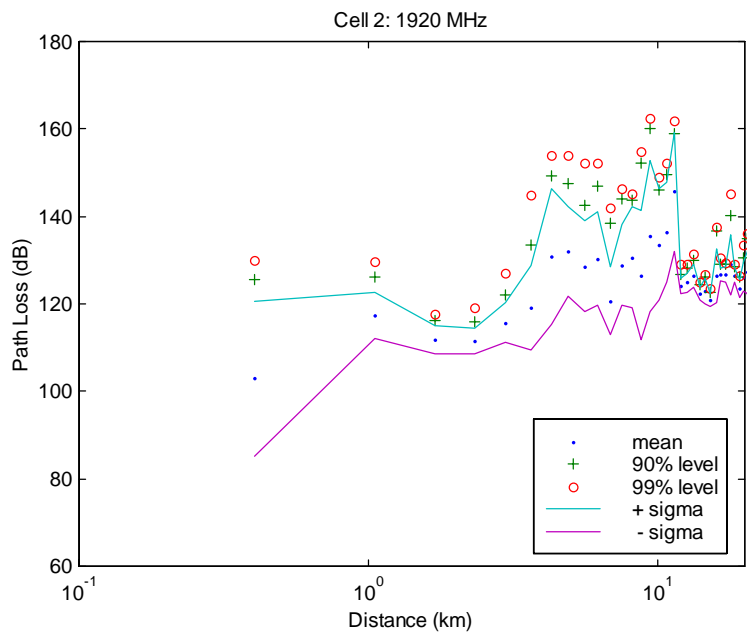


Figure 4.10. Basic transmission loss variance, Cell 2, 1920 MHz.

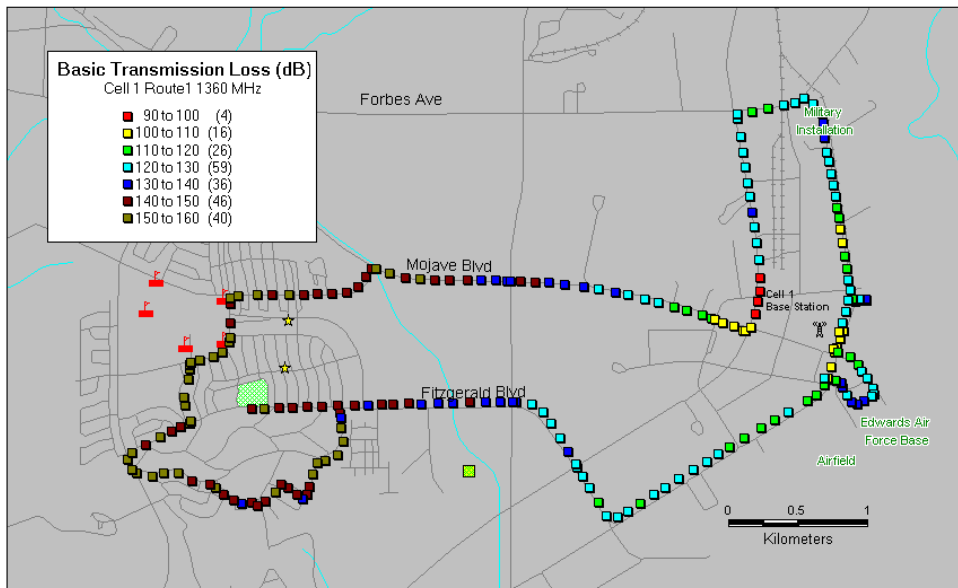
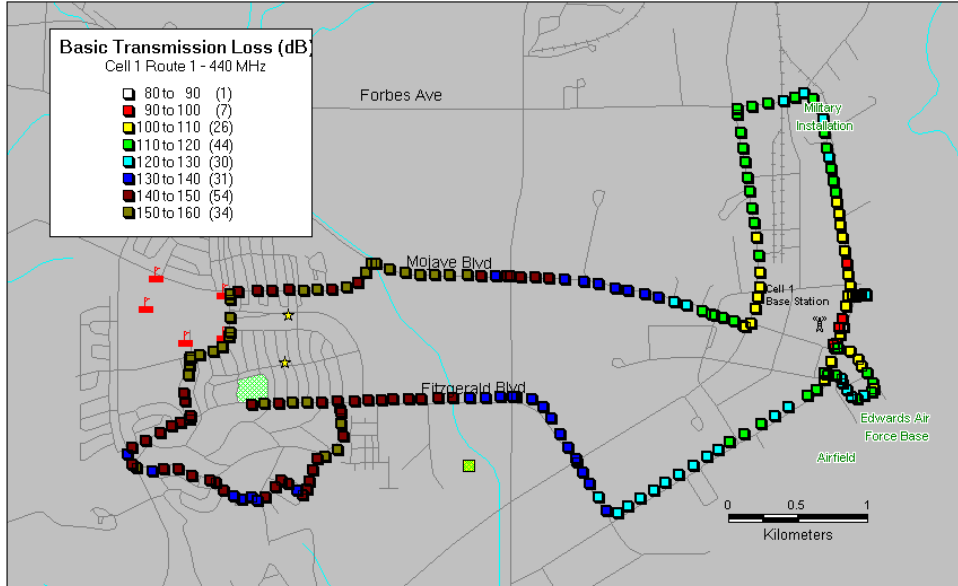


Figure 4.11. Basic transmission loss route map, Cell 1, Route 1, 440 MHz.

Figure 4.12. Basic transmission loss route map, Cell 1, Route 1, 1360 MHz.

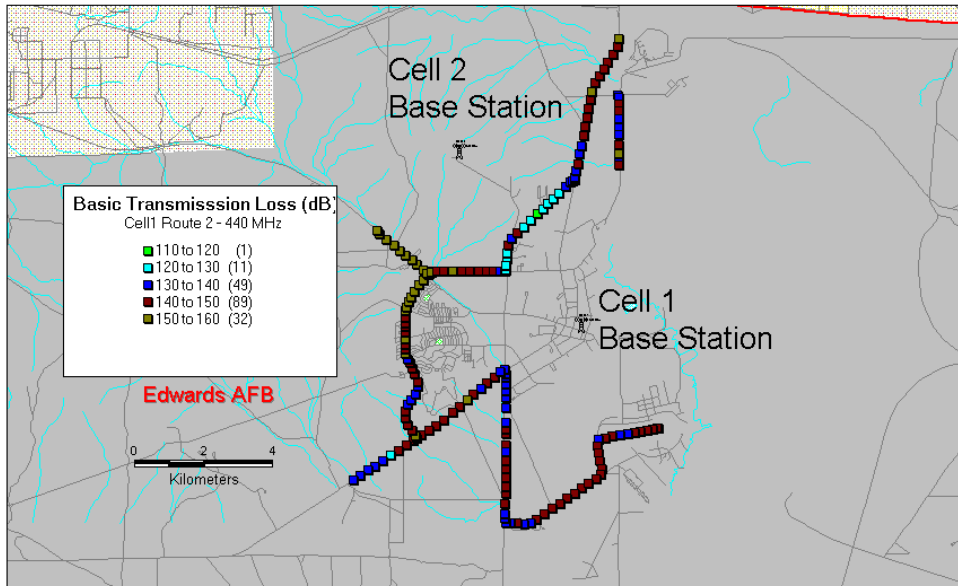
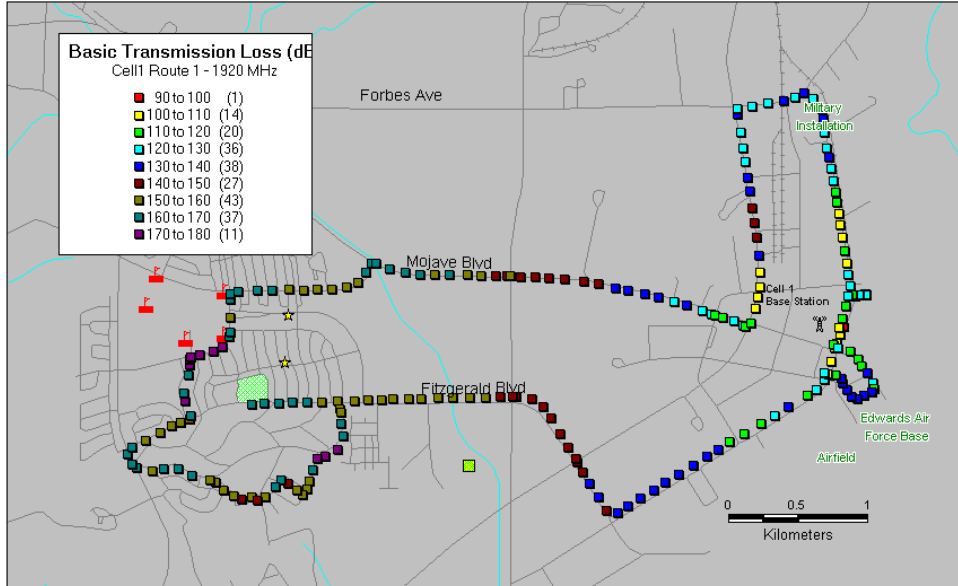


Figure 4.13. Basic transmission loss route map, Cell 1, Route 1, 1920 MHz.

Figure 4.14. Basic transmission loss route map, Cell 1, Route 2, 440 MHz.

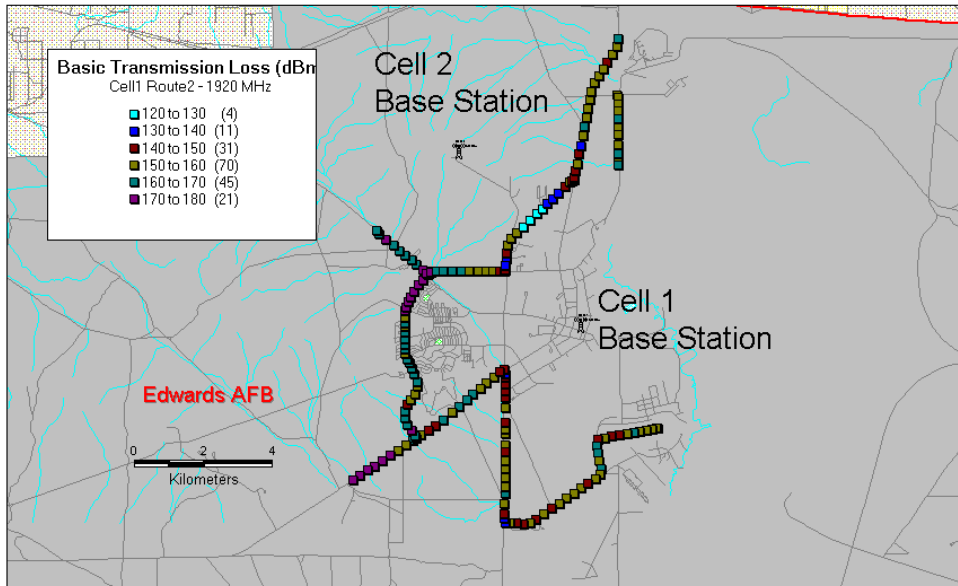
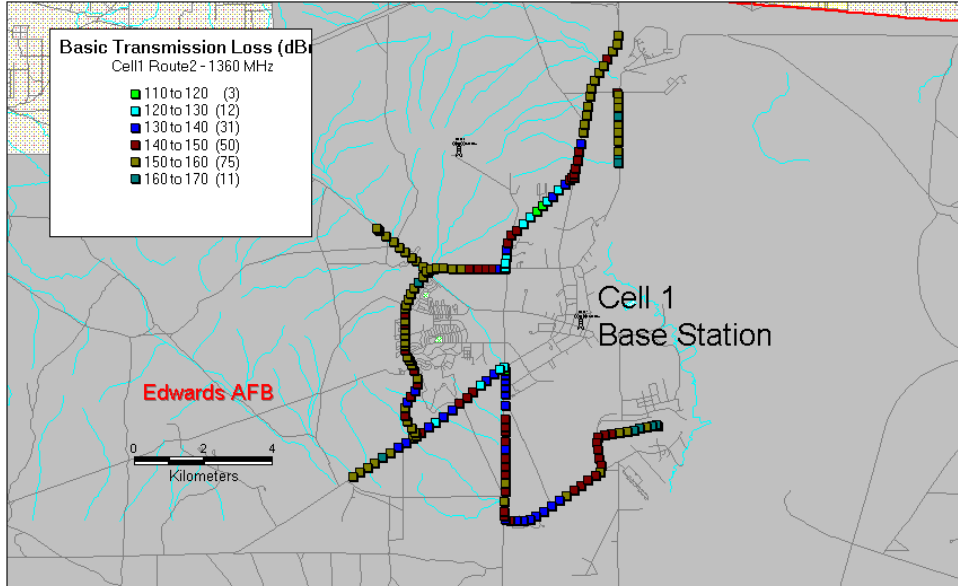


Figure 4.15. Basic transmission loss route map, Cell 1, Route 2, 1360 MHz.

Figure 4.16. Basic transmission loss route map, Cell 1, Route 2, 1920 MHz.

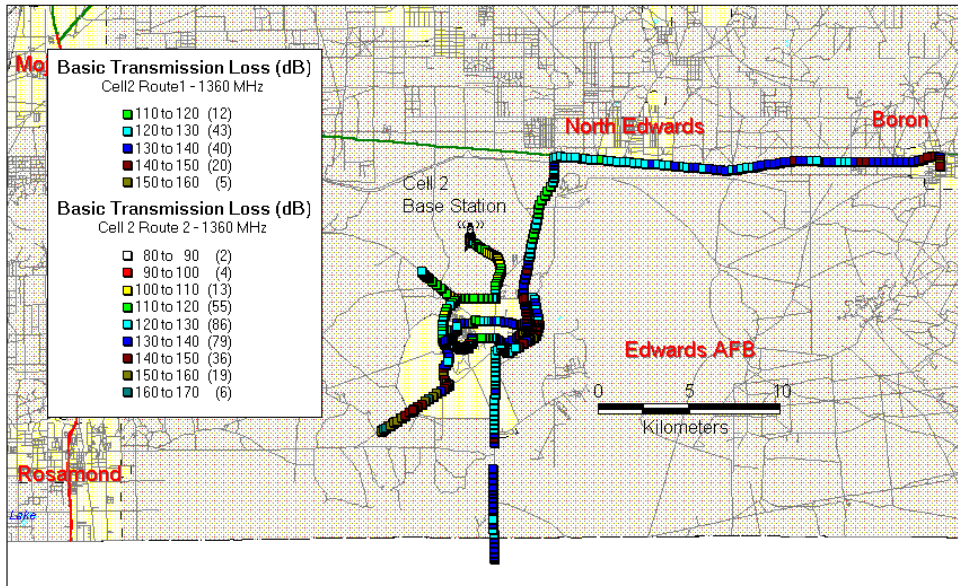
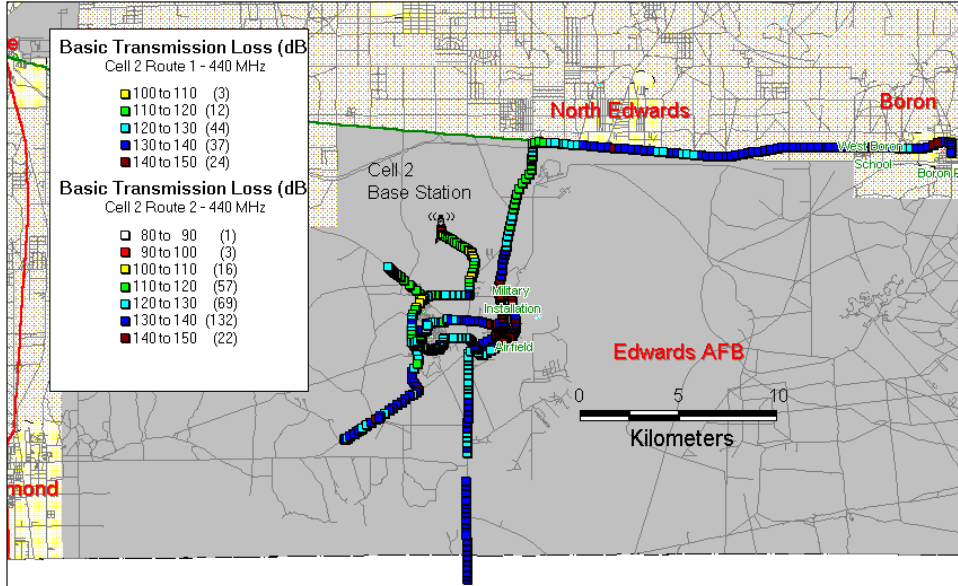


Figure 4.17. Basic transmission loss route map, Cell 2, Routes 1-2, 440 MHz.

Figure 4.18. Basic transmission loss route map, Cell 2, Route 1-2, 1360 MHz.

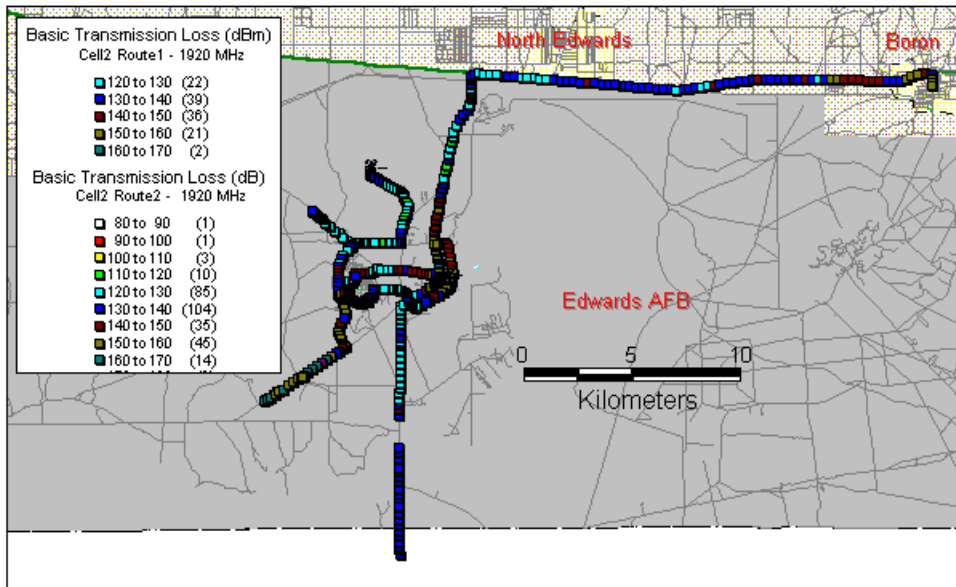


Figure 4.19. Basic transmission loss route map, Cell 2, Routes 1-2, 1920 MHz.

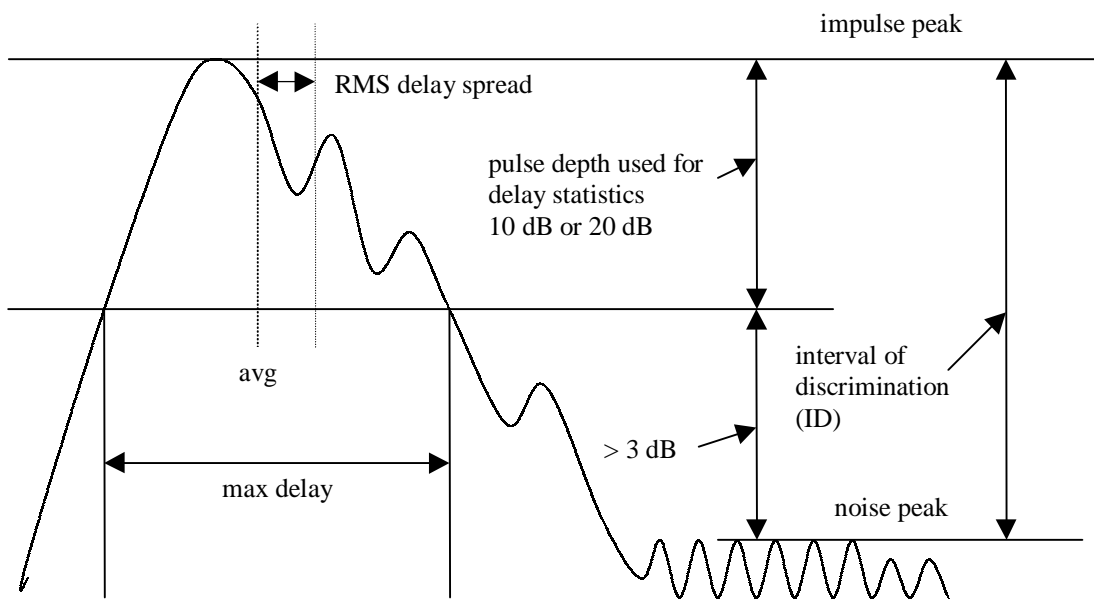


Figure 5.1. Idealized impulse response diagram with descriptive terminology.

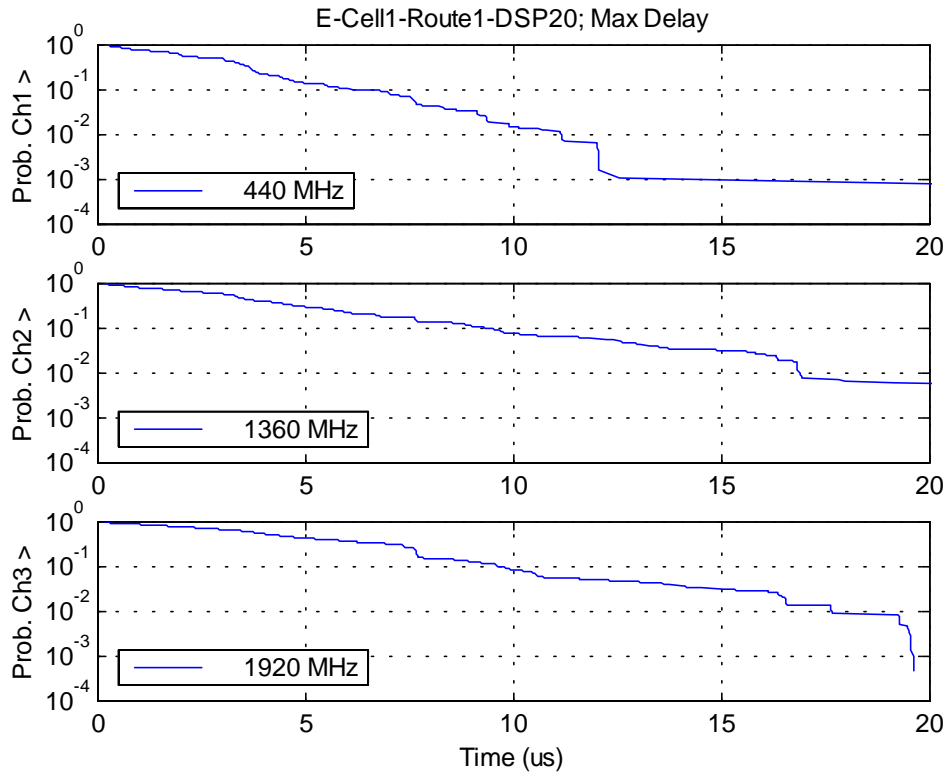


Figure 5.2. Cell 1, Route 1, 20 dB ID: maximum delay CDF.

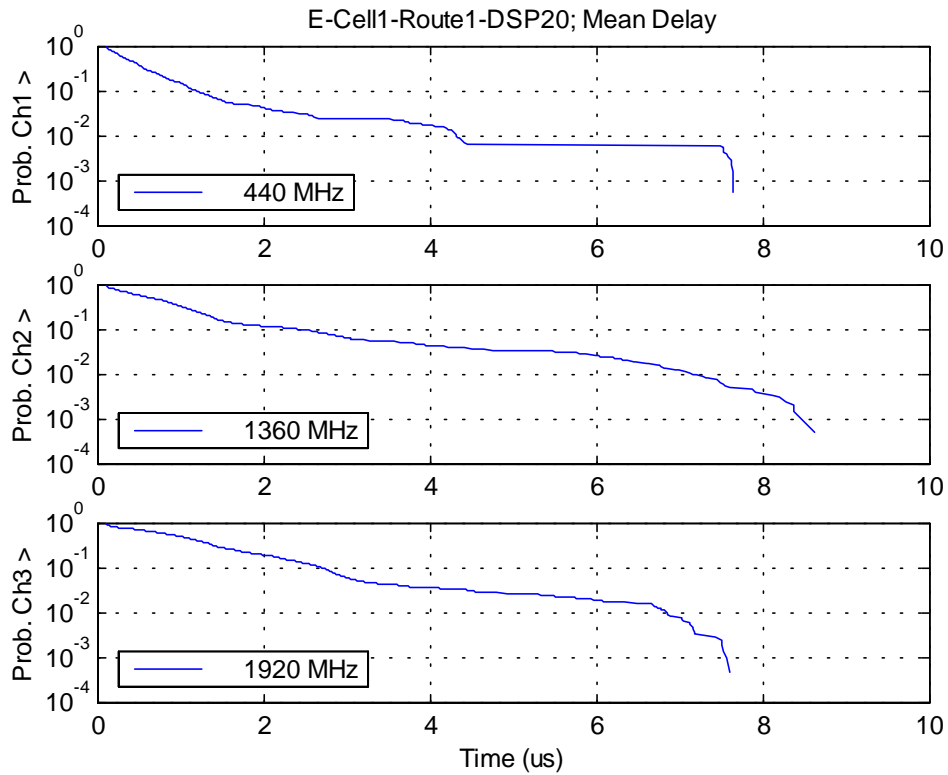


Figure 5.3. Cell 1, Route 1, 20 dB ID: mean delay CDF.

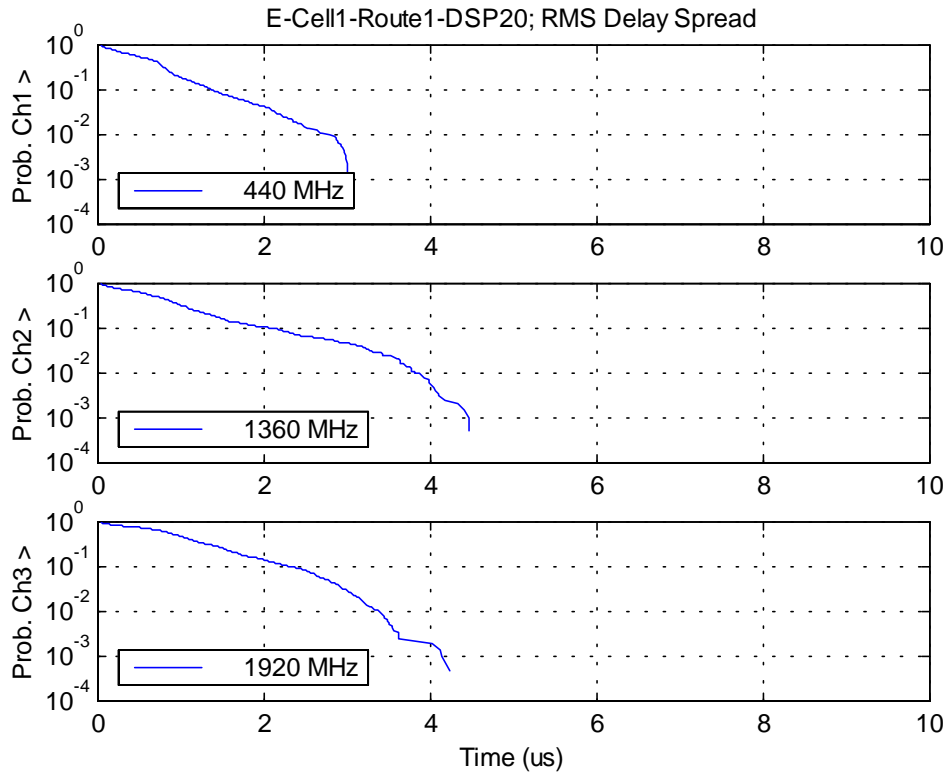


Figure 5.4. Cell 1, Route 1, 20 dB ID: RMS delay spread CDF.

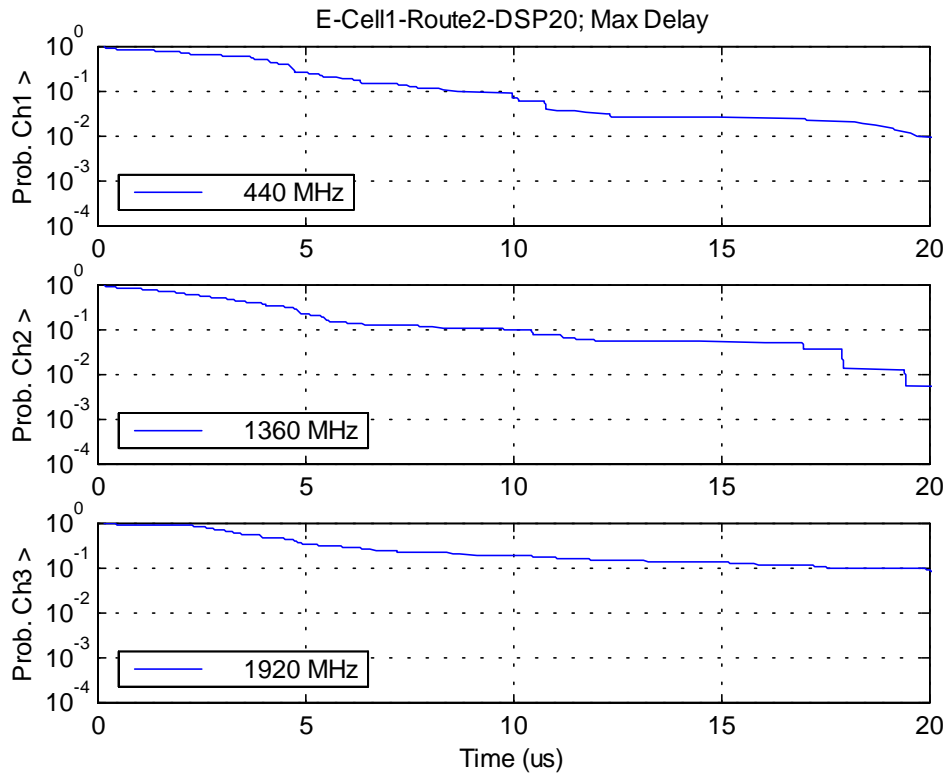


Figure 5.5. Cell 1, Route 2, 20 dB ID: maximum delay CDF.

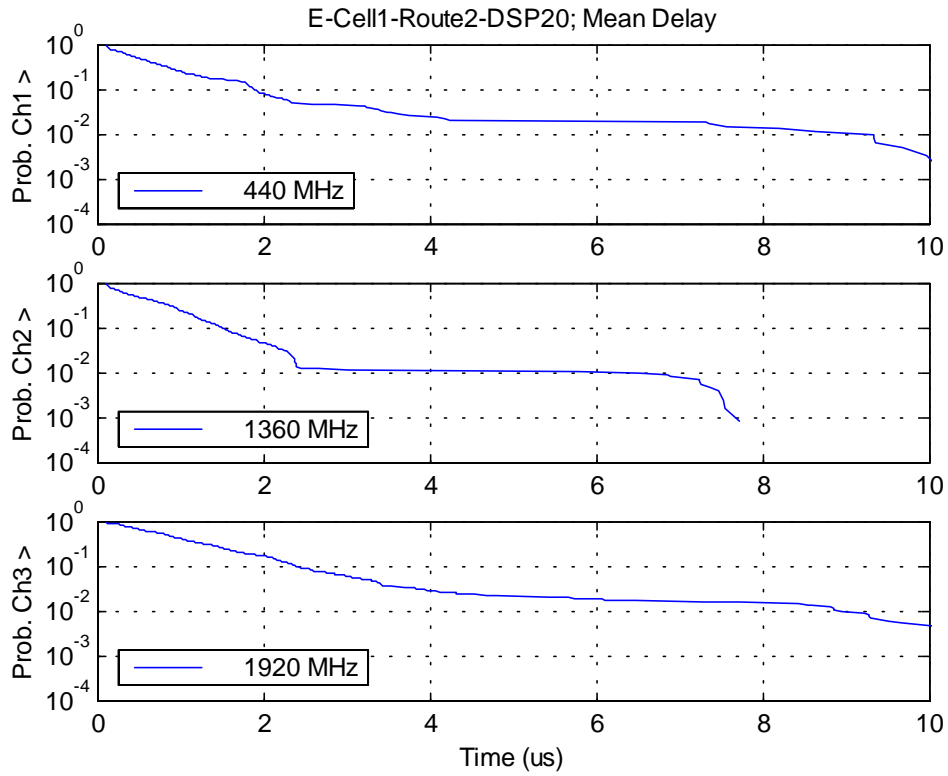


Figure 5.6. Cell 1, Route 2, 20 dB ID: mean delay CDF.

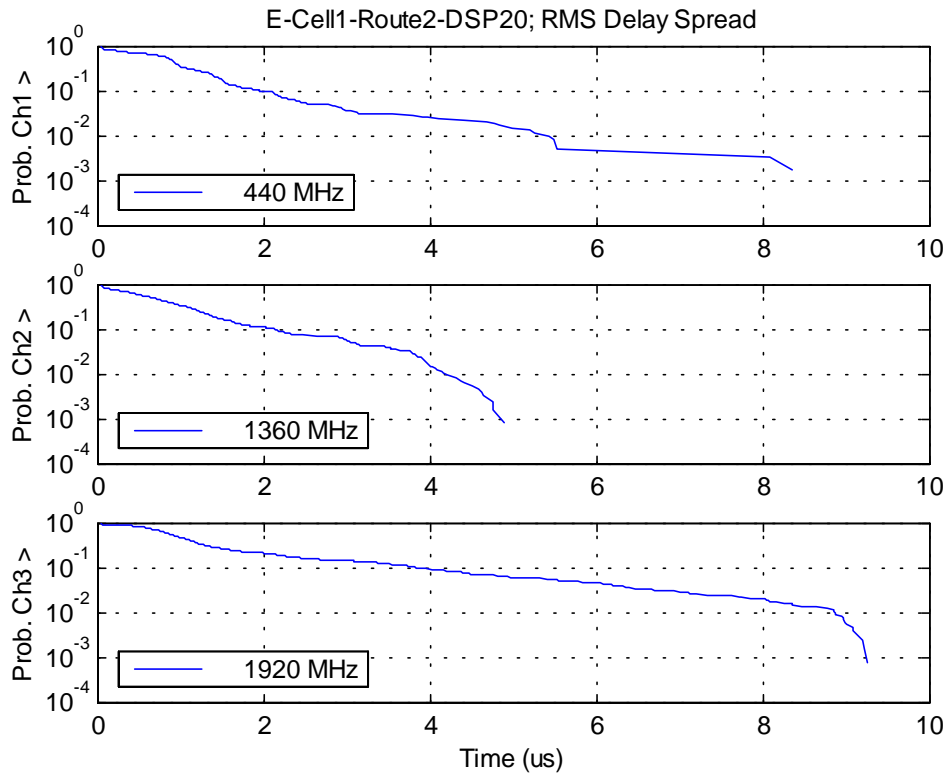


Figure 5.7. Cell 1, Route 2, 20 dB ID: RMS delay spread CDF.

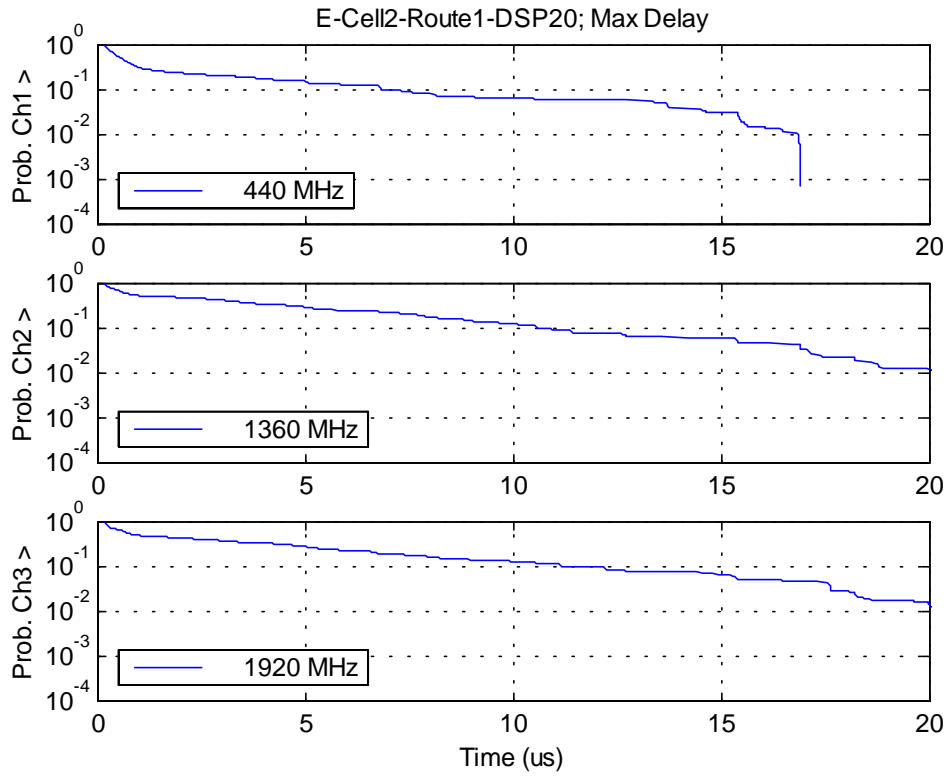


Figure 5.8. Cell 2, Route 1, 20 dB ID: maximum delay CDF.

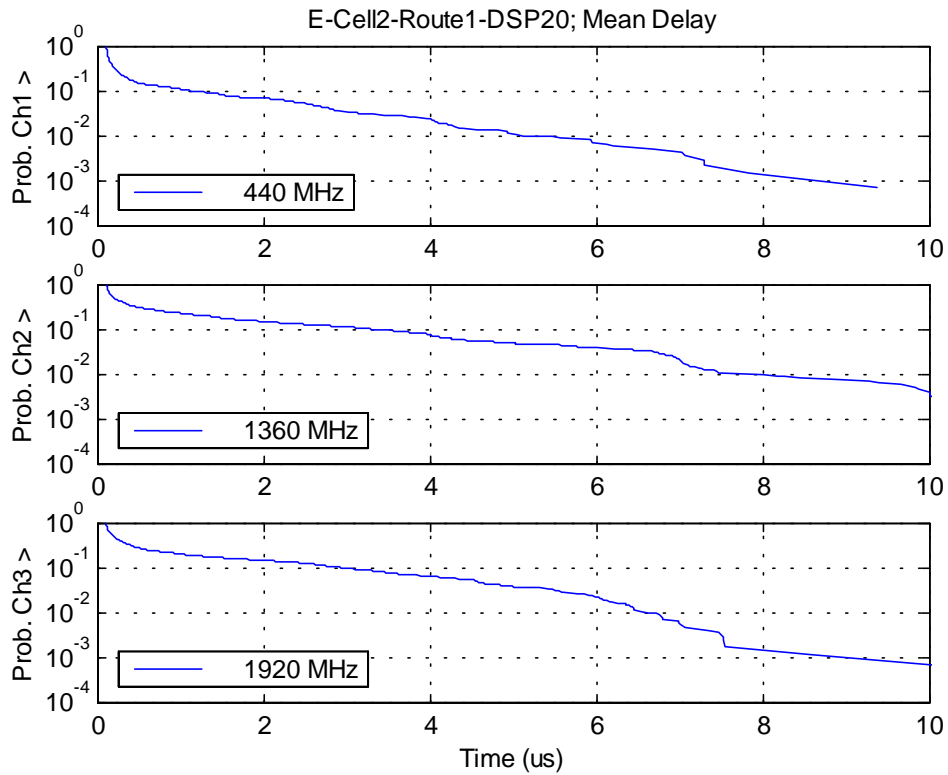


Figure 5.9. Cell 2, Route 1, 20 dB ID: mean delay CDF.

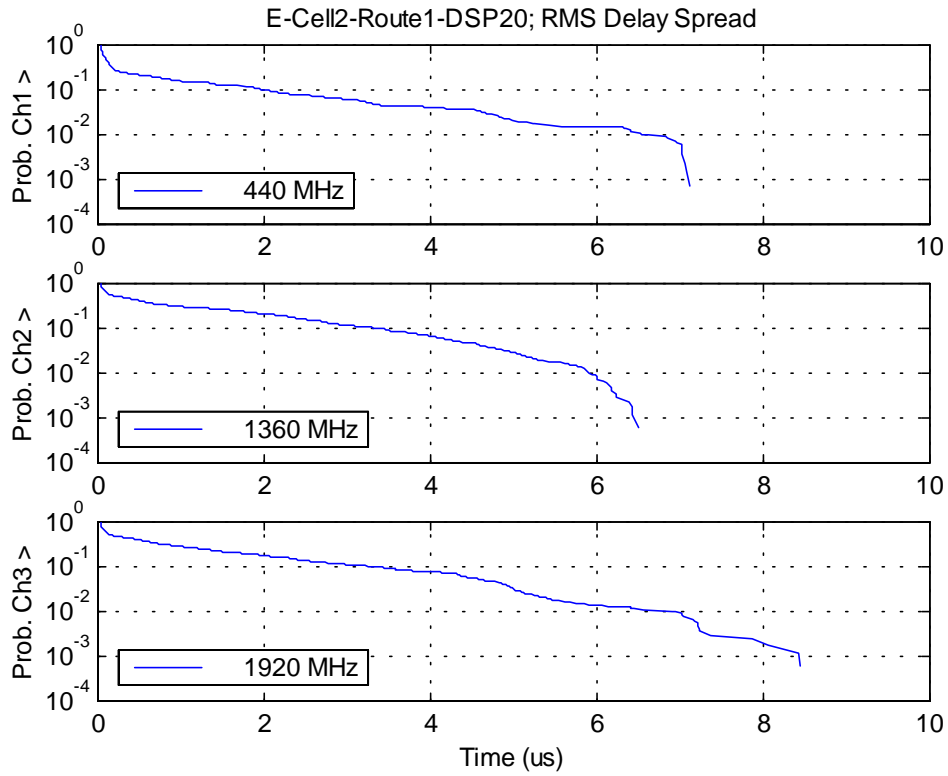


Figure 5.10. Cell 2, Route 1, 20 dB ID: RMS delay spread CDF.

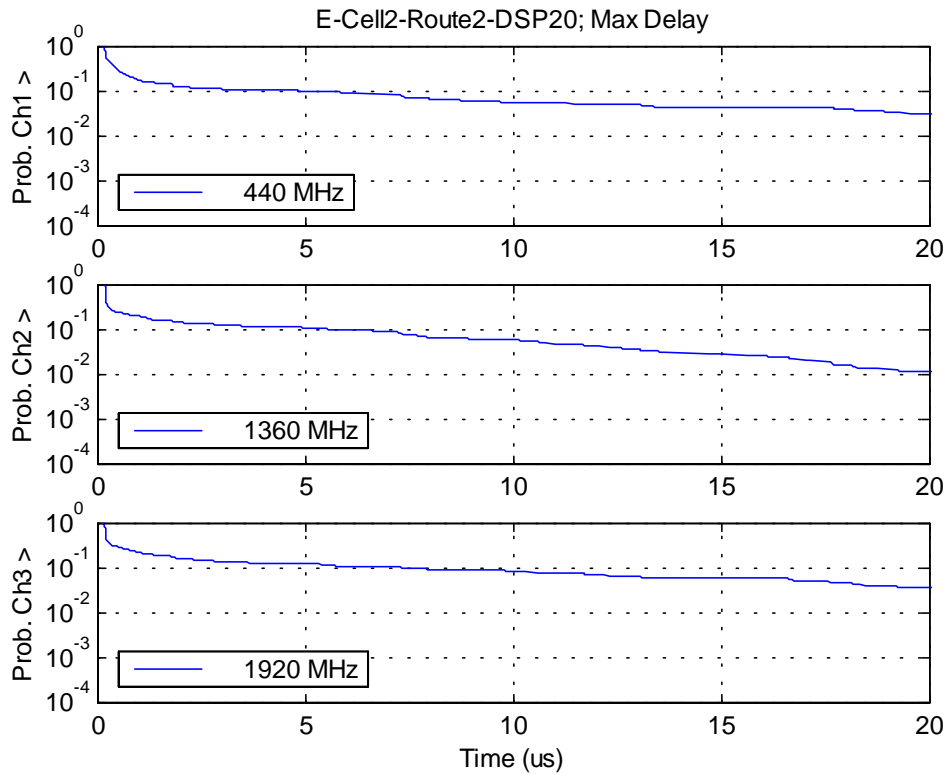


Figure 5.11. Cell 2, Route 2, 20 dB ID: maximum delay CDF.

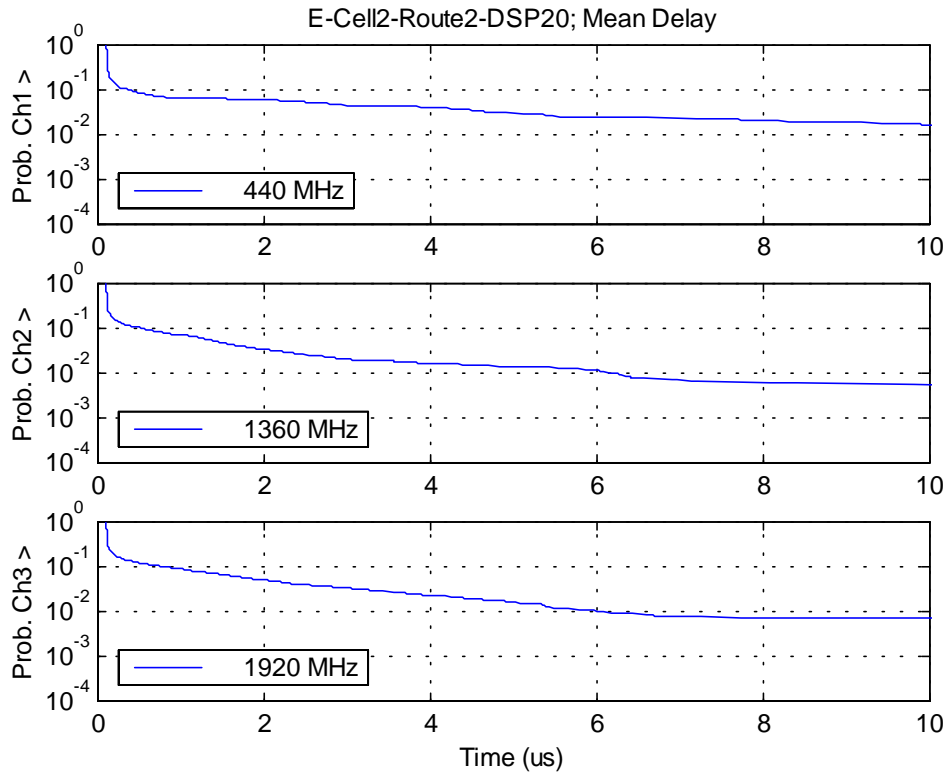


Figure 5.12. Cell 2, Route 2, 20 dB ID: mean delay CDF.

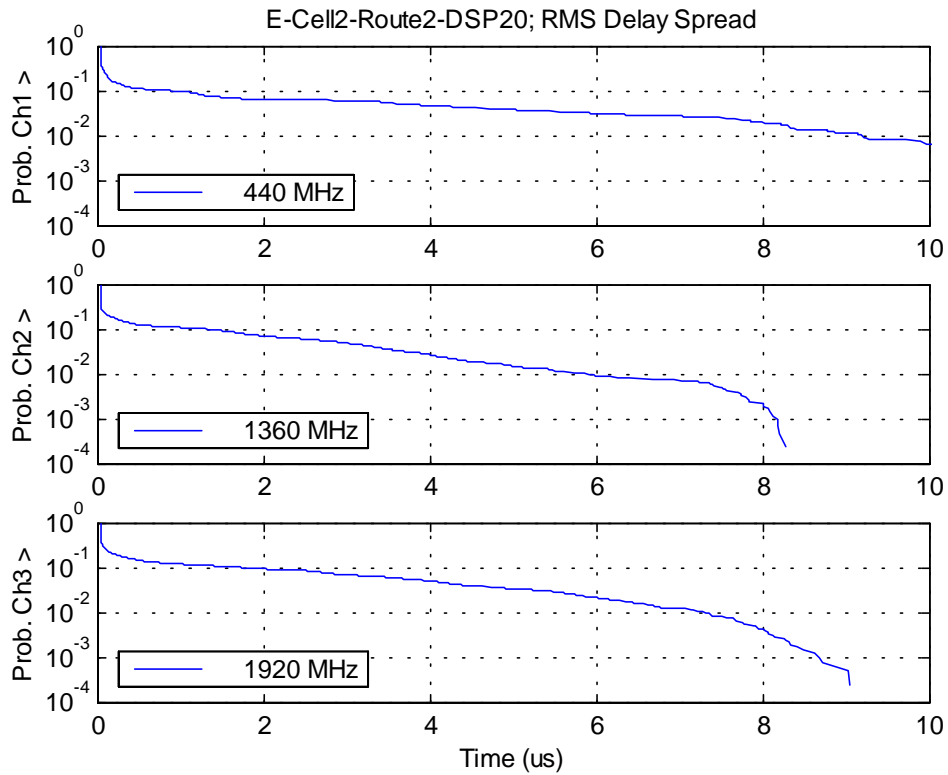


Figure 5.13. Cell 2, Route 2, 20 dB ID: RMS delay spread CDF.

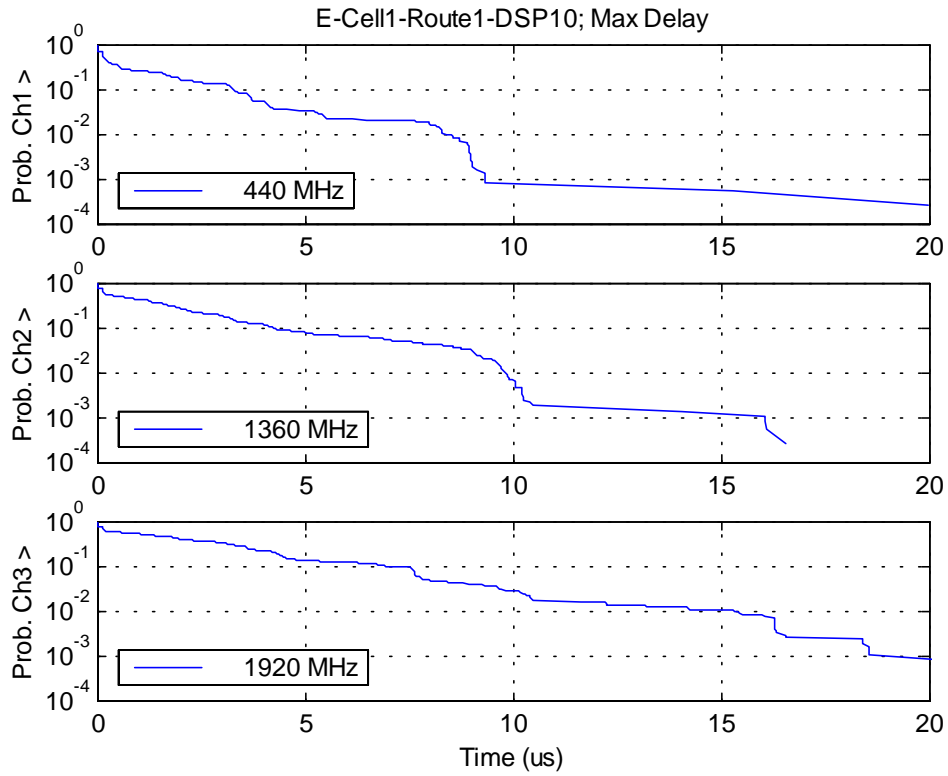


Figure 5.14. Cell 1, Route 1, 10 dB ID: maximum delay CDF.

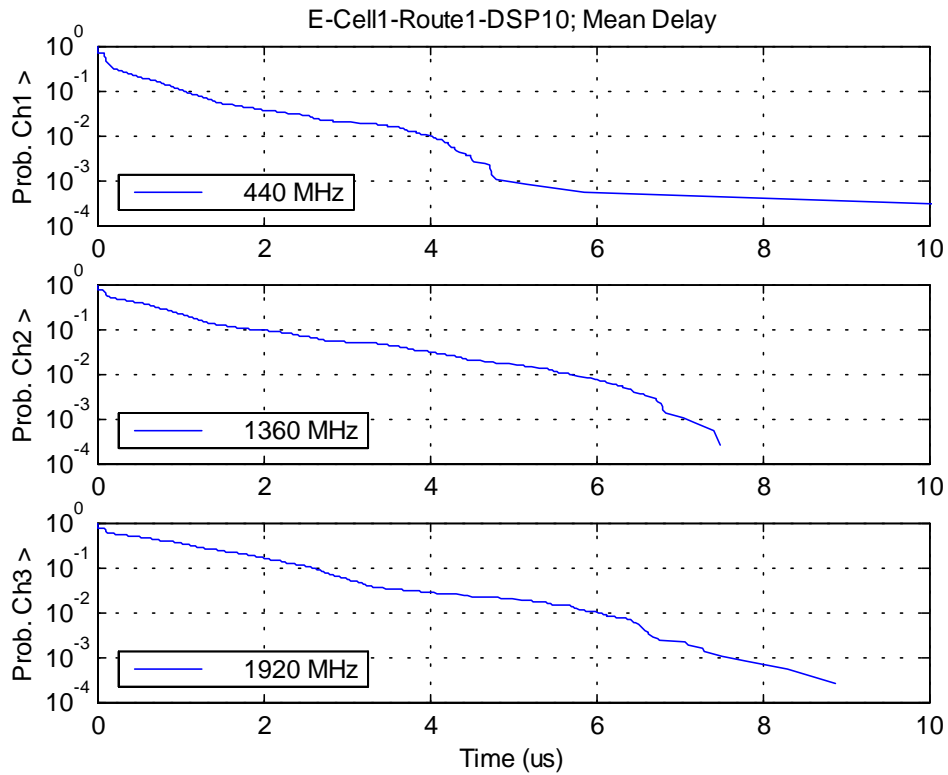


Figure 5.15. Cell 1, Route 1, 10 dB ID: mean delay CDF.

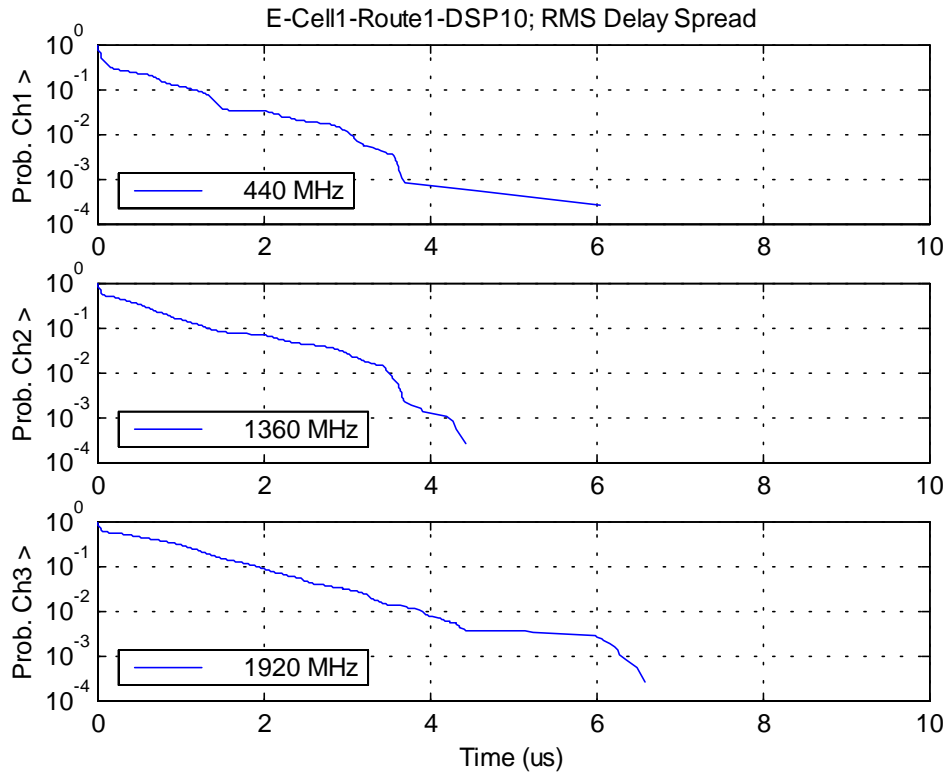


Figure 5.16. Cell 1, Route 1, 10 dB ID: RMS delay spread CDF.

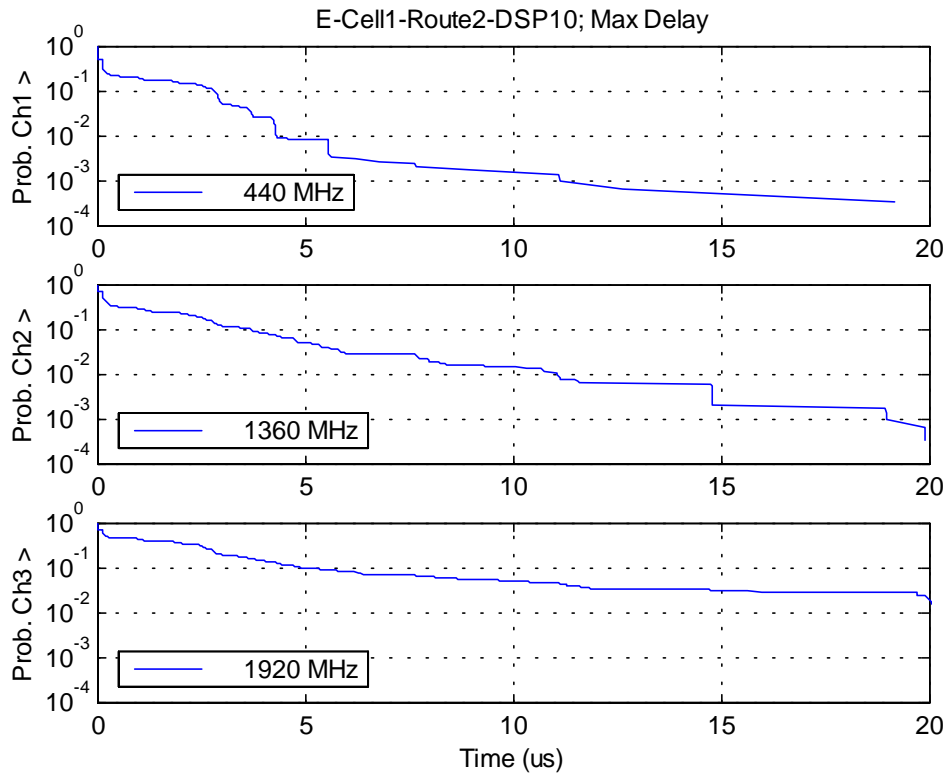


Figure 5.17. Cell 1, Route 2, 10 dB ID: maximum delay CDF.

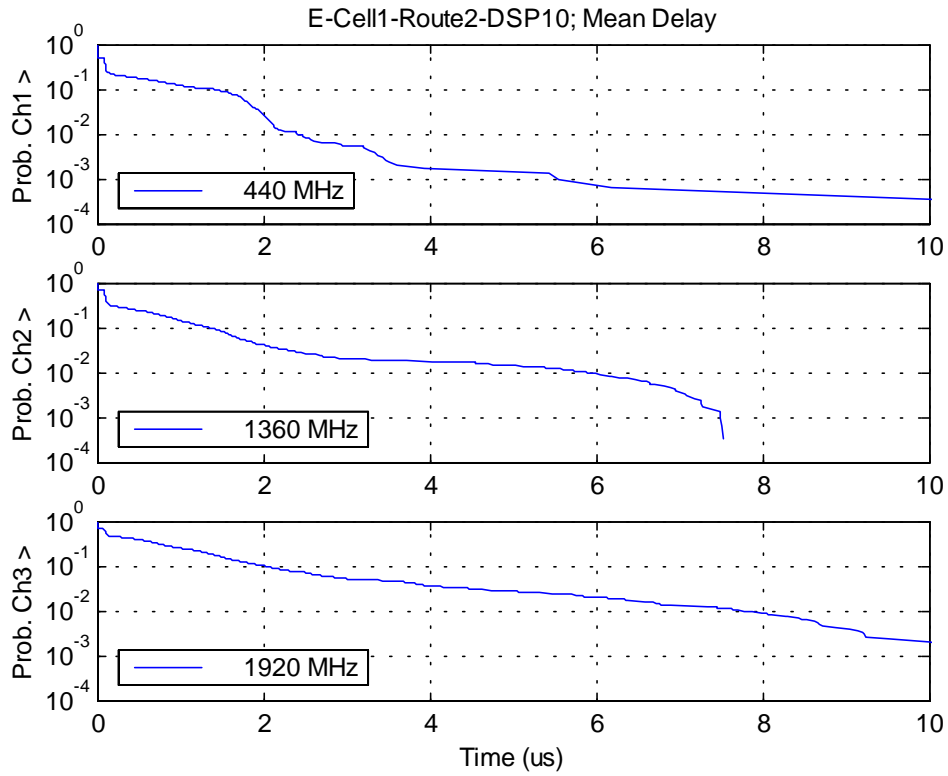


Figure 5.18. Cell 1, Route 2, 10 dB ID: mean delay CDF.

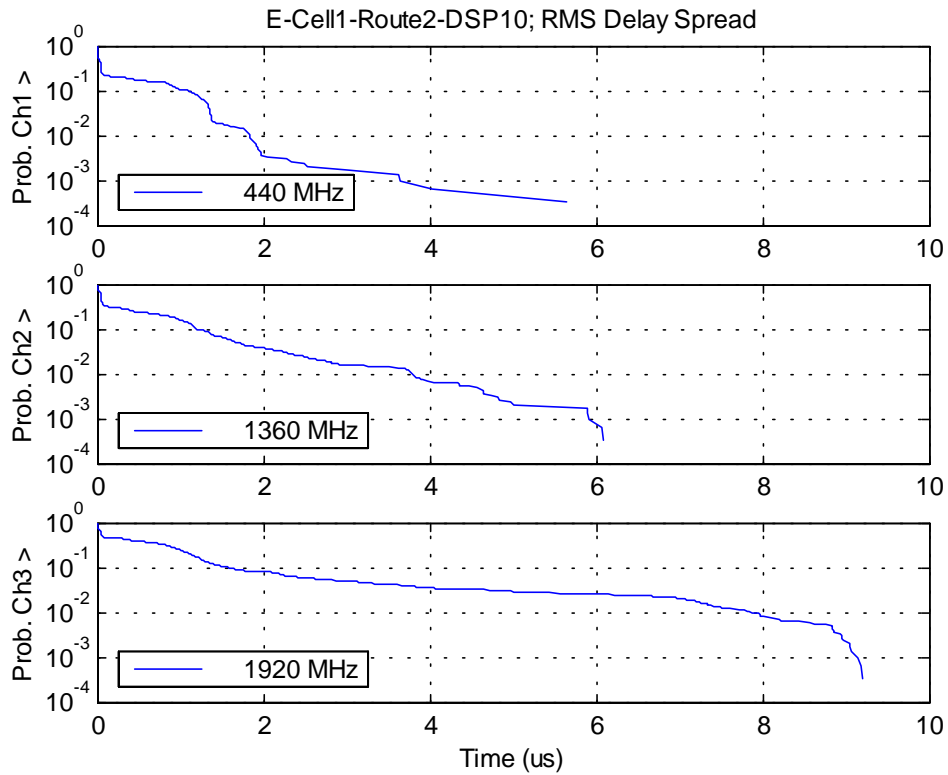


Figure 5.19. Cell 1, Route 2, 10 dB ID: RMS delay spread CDF.

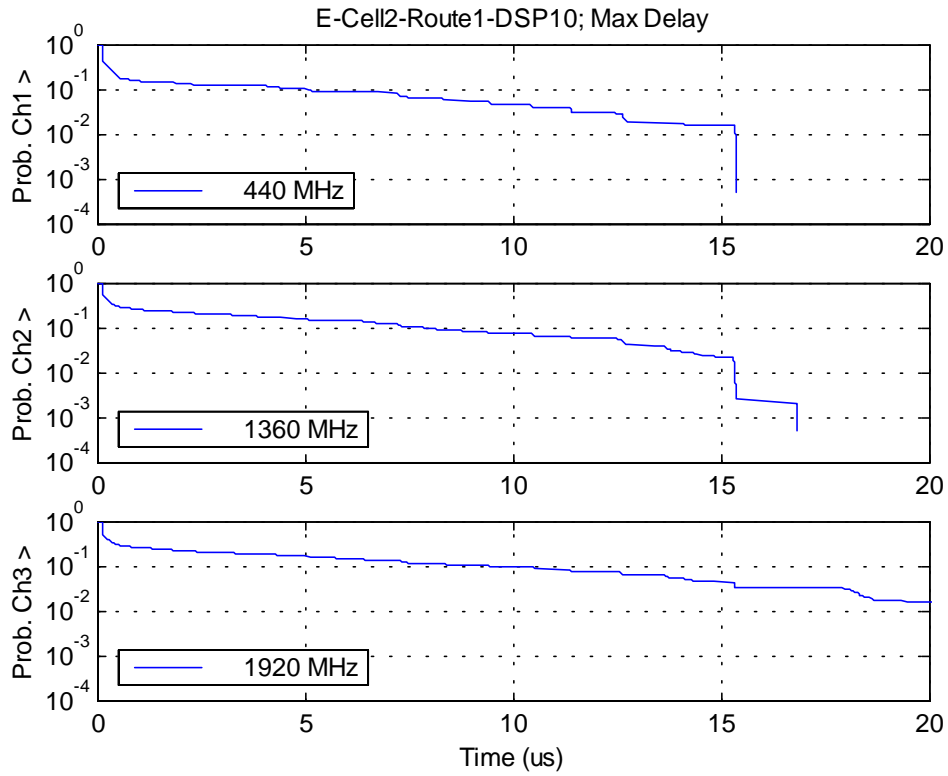


Figure 5.20. Cell 2, Route 1, 10 dB ID: maximum delay CDF.

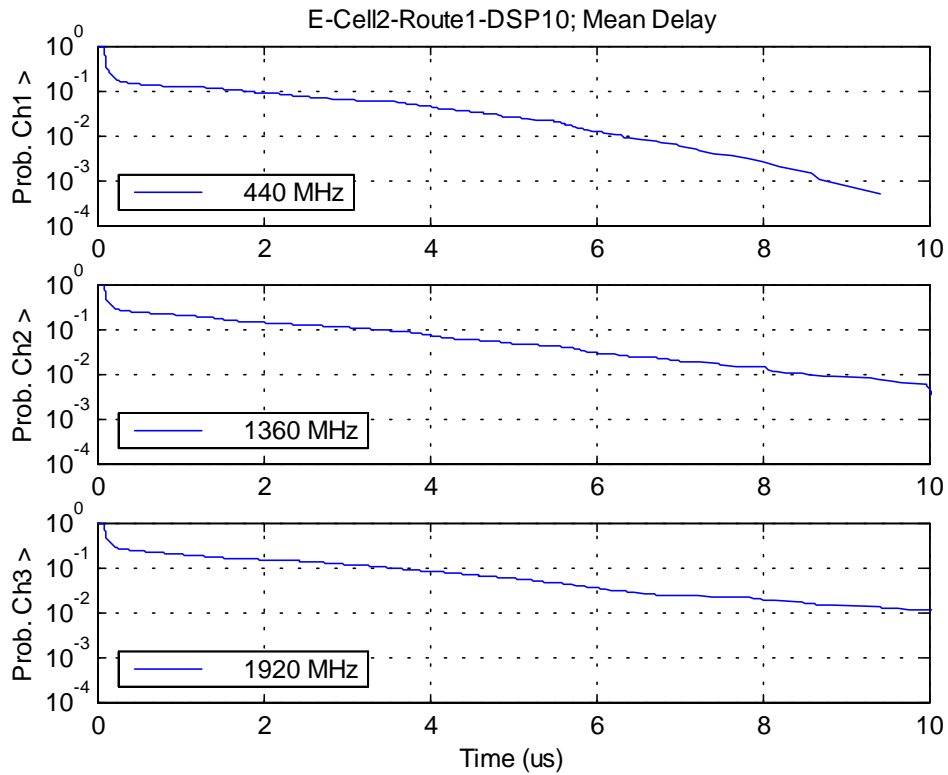


Figure 5.21. Cell 2, Route 1, 10 dB ID: mean delay CDF.

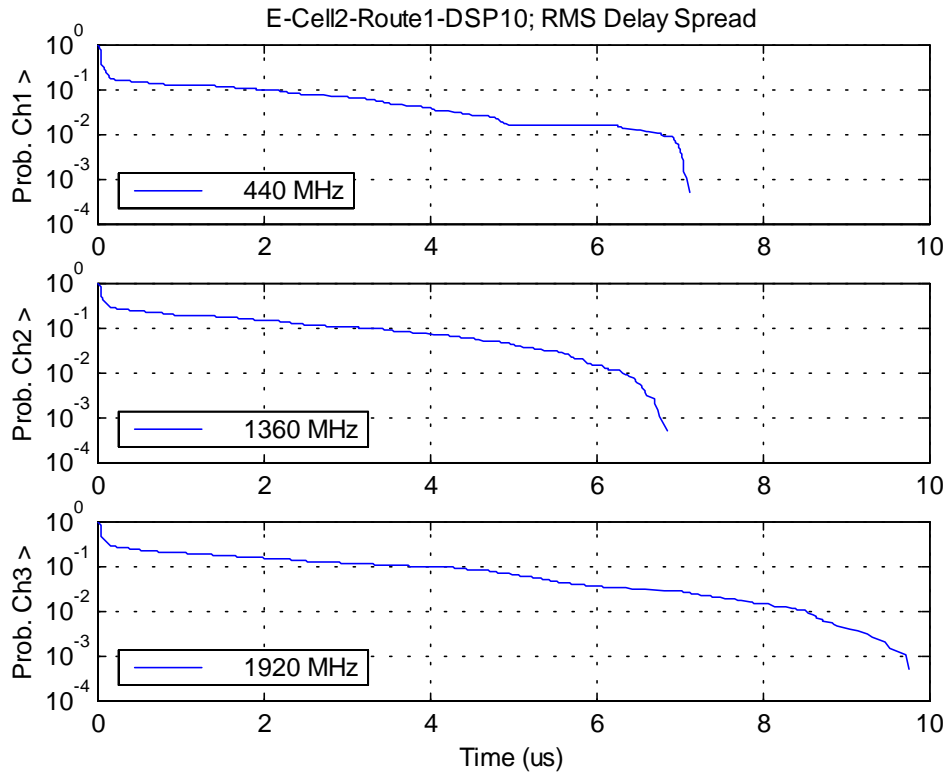


Figure 5.22. Cell 2, Route 1, 10 dB ID: RMS delay spread CDF.

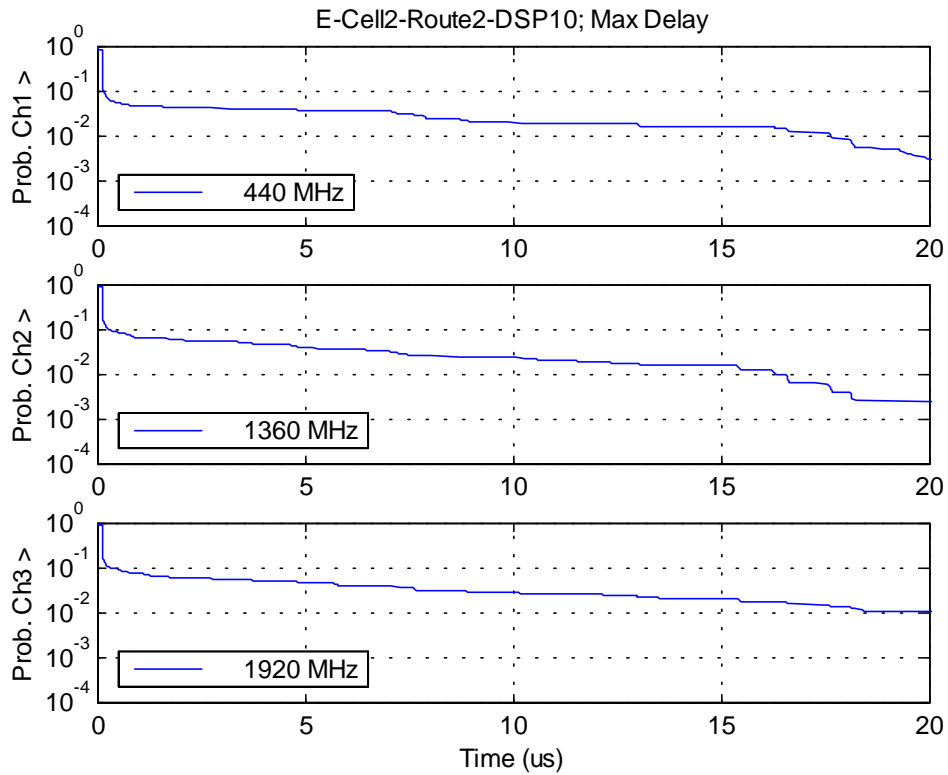


Figure 5.23. Cell 2, Route 2, 10 dB ID: maximum delay CDF.

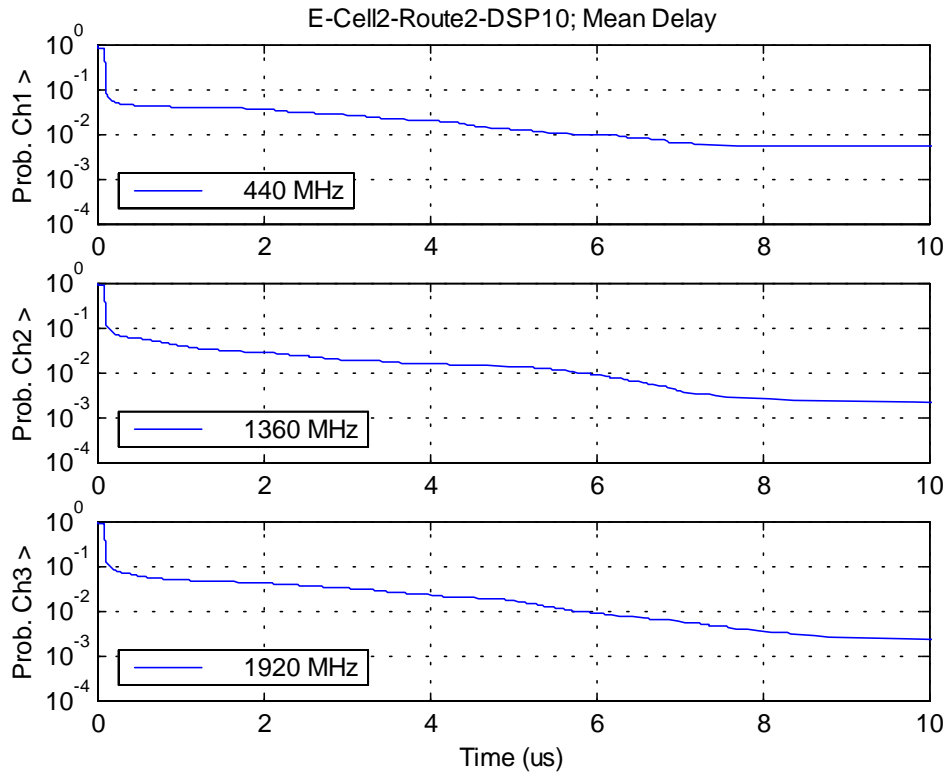


Figure 5.24. Cell 2, Route 2, 10 dB ID: mean delay CDF.

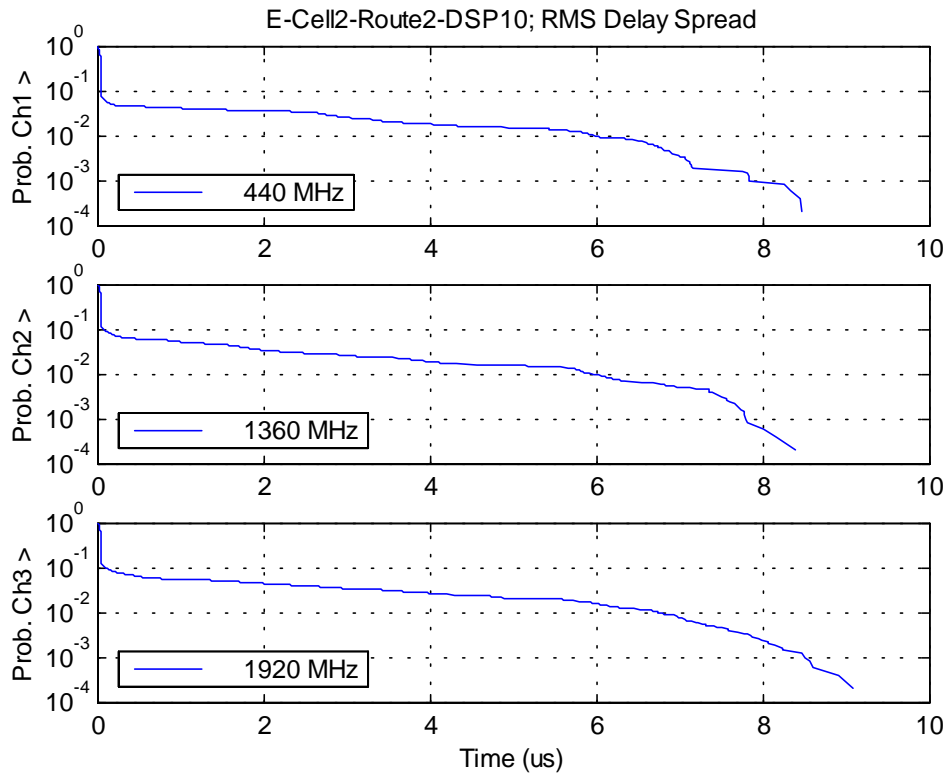


Figure 5.25. Cell 2, Route 2, 10 dB ID: RMS delay spread CDF.

This Page Intentionally Left Blank

This Page Intentionally Left Blank

APPENDIX A: ANTENNA CALIBRATION

The transmitter and receiver antennas were calibrated in a variety of environments. This is especially important for the receive antennas, which were inexpensive monopoles with limited calibration data available from the manufacturers. The 440 MHz transmit dipole also had poor calibration data. The 1360 MHz and 1920 MHz transmit dipole antennas were high quality and had manufacturer’s calibration data which agree with our measurements. Calibrations consisted of two far-field tests which included the measurement vehicle. The third test utilized the NIST anechoic chamber. The NIST test used a circular ground plane for the monopole antennas.

The first far-field test utilized a calibrated EMCO horn antenna for the 1360 MHz and 1920 MHz source and a calibrated Antenna Specialists discone antenna at 440 MHz. The source antenna gains are listed in Table A1.

Table A1. Source Antenna Gain Data used for the Far Field Tests

Frequency(MHz)	Manufacturer	Gain(dBi)
440	Antenna Specialists	14
1360	EMCO	7.5
1920	EMCO	7.8

For this test, transmit antennas were positioned on the roof of wing 4 of the Radio Building and the van was parked east of wing 2 along the south access road. The radio path is approximately 148 m and the elevation difference is 10.4 m. The van was oriented broadside to the transmit antennas at 5 sites 1 m apart. The elevation angle was approximately 4°. Measurements were made on two separate days and averaged. The azimuth pattern of the 1360 MHz transmitter dipole was also measured. Averaged gain measurements for the field trail antennas are summarized in Tables A2 and A3.

Table A2. Gain Measurements for the Receiving Antennas

Frequency(MHz)	Manufacturer	Antenna Gain(dBi) Specification	Antenna Gain(dBi) Measured
440	Larson 5/8 λ monopole	5.2	4.8
1360	Larson 1/4 λ monopole	None	-3.4
1920	Andrew PCS monopole	3	.75

Table A3. Gain Measurements for the Transmitting Antennas

Frequency(MHz)	Manufacturer	Gain(dBi) Specification	Gain(dBi) Measured
440	Cushcraft FRX430 omni directional dipole	5	0.55
1360	Dorne&Margolin DM-Q130-1 directional	12	11.33
1920	Andrew PCS-0190A-006 omni directional	6.9	6.9

Pattern measurements for the D&M antenna are given in Table A4. These results agreed well with the 360° pattern supplied by the manufacturer. The manufacturer's data was used to create a lookup table.

Table A4. 1360 MHz Dorne & Margolin Gain Measurements versus Azimuth Angle

G(0°)	G(90°)	G(180°)	G(270°)
11.3 dBi	7.3 dBi	1.3 dBi	4.3 dBi

A second set of far field tests were made at the ITS Table Mountain site where a 360° azimuth pattern measurement of the receiving antennas and measurement van combination could be made. These tests were made at three distances at an elevation angle of 0°. The source antennas used were the same as in Table A1 except for the 440 MHz measurement which utilized the 440 MHz Cushcraft dipole. The 440 MHz source gain has been adjusted to reflect the calibration of this antenna in the NIST chamber as reported in the last section of this appendix. The average gain measurement over all angles and distances is given in Table A5. Figure A1 is the 360° pattern showing the influence of the van and shadowing by the mast on the roof. On this plot, 0° gives results for the van pointed head on to the calibration antenna. Also included are results for a 1360 MHz trailer mounted antenna.

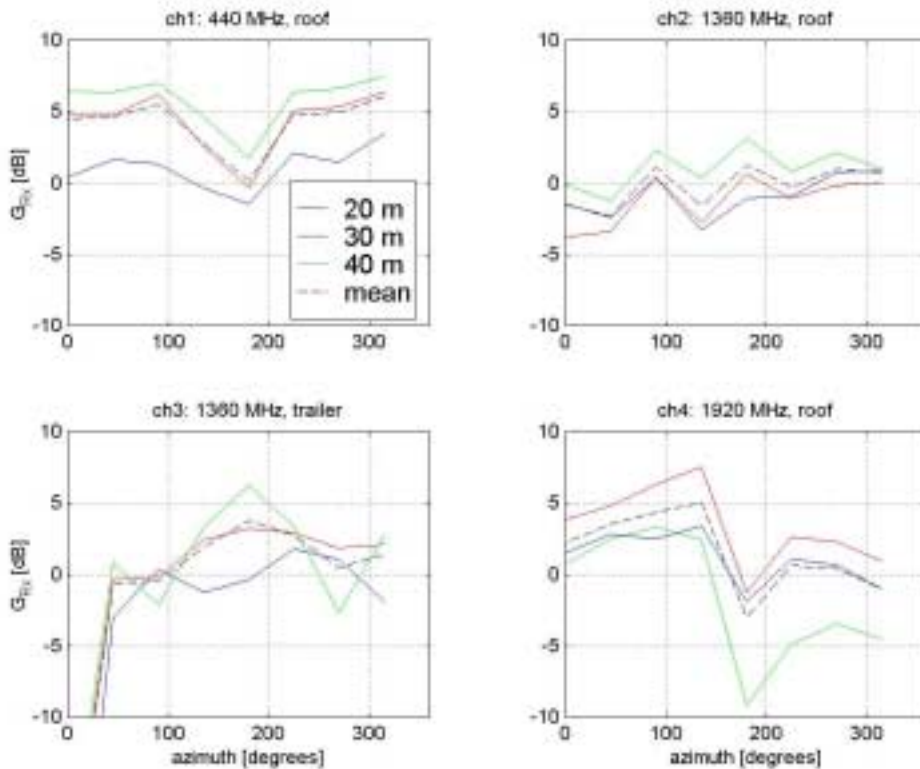


Figure A1. Antenna patterns measured at Table Mountain showing gain above isotropic versus van azimuth.

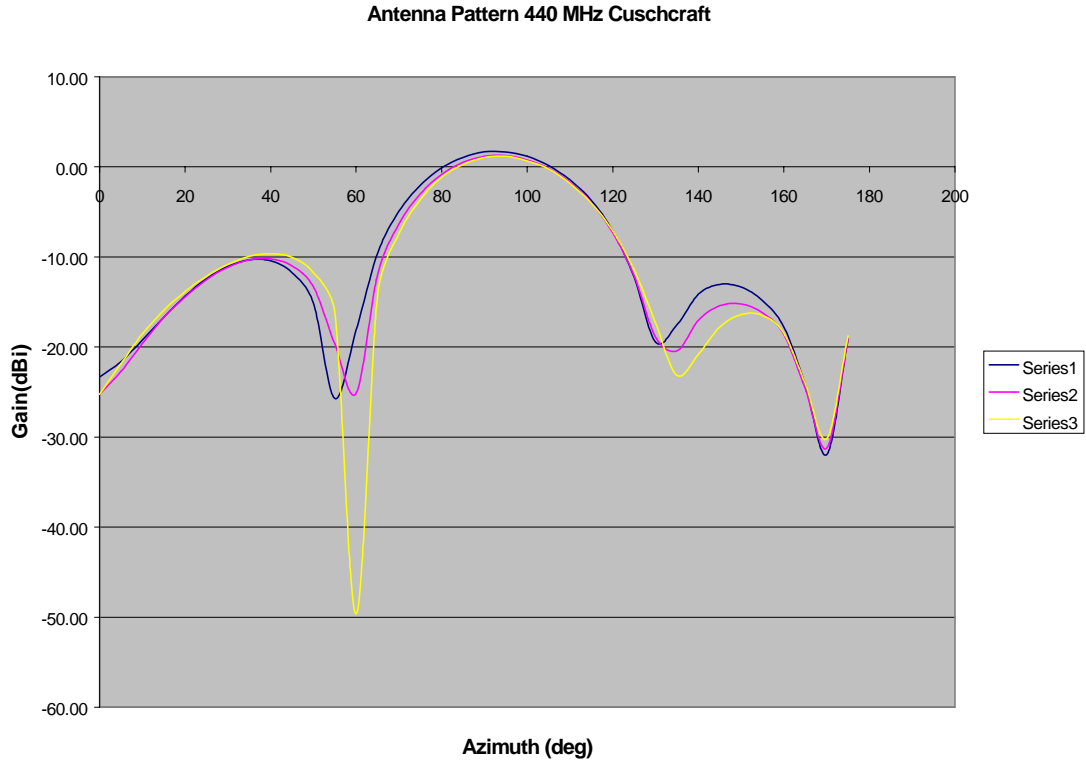


Figure A2. Gain of 440 MHz Cushcraft transmitter dipole (NIST Chamber).

Table A5. Averaged Table Mountain Azimuth Gain Measurements

Frequency(MHz)	Manufacturer	Mounting	Average Gain(dBi) Measured
440	Larson $5/8 \lambda$ monopole	Roof	4.1
1360	Larson $1/4 \lambda$ monopole	Roof	-0.2
1360	Larson $1/4 \lambda$ monopole	Trailer	-1.7
1920	Andrew PCS monopole	Roof	1.5

The Table Mountain measurements show the effects of the measurement van, shadowing and multipath from the ground reflection. The roof mounted antennas were shadowed by the van mast at about 180° . This produced a 3 to 5 dB drop for about 10 % of the pattern for the 440 MHz roof antenna. The 1360 MHz roof antenna has about 3 dB variability but no apparent shadowing. The 1920 MHz roof antenna has 5 to 10 dB shadowing effects for about 10% of the pattern and 3 dB variability. The 1360 MHz trailer antenna has a 10 dB drop between 0° and 20° , or about 10% of the pattern.

A third set of measurements was completed in the NIST anechoic chamber. A 1.3 m circular ground plane was utilized with the monopole receiving antennas and the vertical pattern was measured. The vertical pattern of the 440 MHz Cushcraft transmit dipole was

also measured with no ground plane. Figures A2-A5 show the patterns for the three receiving antennas and Table A6 lists the measured antenna gains.

The gain of the 440 MHz Cushcraft dipole has a broad maximum near 90 degrees (on the horizon). The monopole antenna measurement plane puts 0° on the horizon. Gain for these antennas peak between 15° to 20° although the Larson 5/8 λ monopole has a broad peak near the horizon. The gain versus angle is given in Table A6.

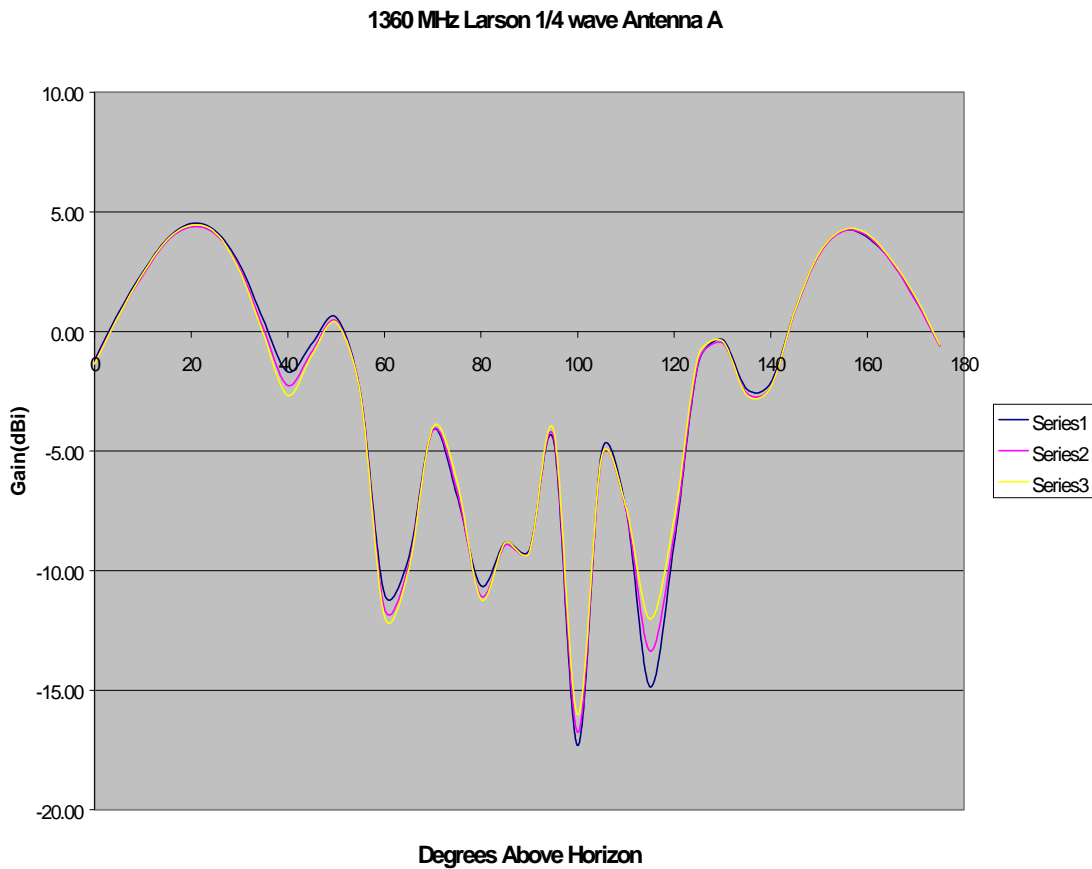


Figure A3. 1360 MHz Larson receiving monopole pattern (NIST Chamber).

Table A6. Gain Measured in the NIST Anechoic Chamber for the Receiving Monopole Antenna

F(MHz)	Gain(dBi)											
	Larson 440 MHz			Larson 1360 MHz			Andrew 1920 MHz			Cushcraft 440 MHz		
Elevation Angle (deg)	435	440	445	1355	1360	1365	1915	1920	1925	435	440	445
0	1.8	1.1	0.8	-1.2	-1.3	-1.4	-0.6	-0.7	-0.9	-23.3	-25.2	-25.2
5	2.4	1.9	1.6	0.8	0.7	0.7	1.5	1.4	1.2	-21.6	-22.7	-21.9
10	2.8	2.3	2.0	2.5	2.4	2.4	3.0	2.9	2.7	-19.2	-19.6	-18.6
15	2.7	2.2	2.0	3.9	3.8	3.8	3.6	3.5	3.3	-16.7	-16.7	-15.9
20	1.9	1.5	1.4	4.5	4.4	4.4	2.7	2.7	2.4	-14.4	-14.4	-13.8
25	0.5	0.1	0.1	4.2	4.1	4.1	-0.4	-0.5	-0.6	-12.4	-12.5	-12.1
30	-2.2	-2.4	-2.1	2.8	2.6	2.5	-8.0	-7.7	-7.5	-11.0	-11.1	-10.8
35	-6.3	-5.8	-5.0	0.4	0.1	-0.2	-8.5	-8.3	-8.3	-10.3	-10.3	-9.9
40	-9.7	-8.2	-6.7	-1.7	-2.3	-2.7	-3.1	-3.1	-3.2	-10.4	-10.2	-9.6
45	-6.3	-6.2	-5.5	-0.5	-0.8	-1.0	-1.7	-1.9	-2.1	-11.7	-11.0	-10.0
50	-3.4	-3.9	-3.9	0.6	0.4	0.4	-3.8	-3.9	-4.0	-15.1	-13.3	-11.7
55	-1.9	-2.8	-3.2	-2.5	-2.6	-2.6	-0.7	-0.7	-0.7	-25.7	-19.6	-16.1
60	-1.6	-2.8	-3.3	-11.0	-11.6	-11.9	-1.9	-2.2	-2.5	-18.1	-25.1	-49.6
65	-2.2	-3.5	-4.3	-9.5	-9.8	-10.0	-4.3	-4.4	-4.7	-9.6	-11.9	-14.2
70	-3.4	-4.9	-5.9	-4.1	-4.1	-4.0	-1.8	-1.7	-1.7	-4.9	-6.3	-7.4
75	-5.5	-7.0	-8.2	-6.8	-6.6	-6.2	-9.2	-9.7	-10.3	-2.0	-3.0	-3.6
80	-9.0	-10.6	-11.9	-10.6	-11.1	-11.2	-11.2	-11.6	-12.0	-0.1	-0.8	-1.2
85	-15.7	-17.6	-19.0	-8.8	-8.9	-8.8	-4.7	-4.8	-4.9	1.1	0.5	0.3
90	-22.1	-23.1	-24.1	-9.1	-9.2	-9.2	-4.3	-4.3	-4.3	1.7	1.2	1.1
95	-11.5	-12.9	-13.9	-4.5	-4.4	-4.1	-4.5	-4.4	-4.4	1.6	1.3	1.2
100	-6.9	-8.3	-9.3	-17.3	-16.8	-16.0	-11.1	-11.6	-12.2	1.2	0.8	0.7
105	-4.4	-5.6	-6.4	-5.0	-5.3	-5.2	-2.4	-2.4	-2.3	0.2	-0.2	-0.2
110	-2.8	-3.9	-4.5	-7.4	-7.4	-7.3	-2.5	-2.4	-2.5	-1.4	-1.7	-1.8
115	-2.0	-2.8	-3.1	-14.9	-13.4	-12.0	-2.1	-2.3	-2.5	-3.8	-4.0	-4.1
120	-1.9	-2.5	-2.6	-8.9	-8.5	-7.8	-0.3	-0.2	-0.2	-7.2	-7.3	-7.1
125	-2.9	-3.2	-3.0	-1.3	-1.3	-1.0	-1.4	-1.3	-1.3	-12.3	-12.1	-11.4
130	-5.3	-5.0	-4.3	-0.3	-0.5	-0.4	-0.4	-0.5	-0.7	-19.5	-18.9	-17.3
135	-9.0	-7.5	-5.9	-2.4	-2.6	-2.7	-0.6	-0.7	-0.9	-17.6	-20.4	-23.1
140	-7.7	-6.4	-5.2	-2.1	-2.3	-2.3	-4.3	-4.1	-4.0	-14.1	-17.0	-20.8
145	-3.0	-2.9	-2.5	0.9	0.8	0.9	-5.2	-4.9	-4.6	-13.1	-15.4	-17.8
150	0.1	-0.1	0.0	3.2	3.2	3.3	-0.7	-0.6	-0.6	-13.3	-15.2	-16.4
155	2.0	1.7	1.6	4.2	4.2	4.3	2.1	2.0	1.9	-14.9	-16.2	-16.5
160	3.1	2.6	2.5	3.9	4.0	4.1	3.4	3.2	3.1	-17.8	-18.6	-18.5
165	3.4	2.9	2.7	2.9	2.9	3.0	3.9	3.7	3.5	-24.3	-24.7	-24.1
170	3.3	2.7	2.5	1.3	1.3	1.4	3.8	3.7	3.5	-31.9	-31.2	-30.2
175	2.8	2.2	1.9	-0.6	-0.6	-0.6	3.0	2.9	2.8	-19.0	-19.1	-18.7

The gain on the horizon (0°) as measured in the anechoic chamber was used for data reduction. Data from the chamber for the Cushcraft 440 MHz dipole also was used. The azimuthal pattern for the 1360 MHz dipole was used when reducing the data. This pattern was obtained from the manufacturer and also verified by measurements. Table A7 and Table A8 give the gain and azimuth patterns used for data reduction.

Table A7. Receiving Antenna Gain

Receive Antenna Gains			
Frequency(MHz)	Manufacturer	Gain (dBi)	Azimuth Pattern
440	Larson	1.2	Omni
1360	Larson	-1.3	Omni
1920	Andrew	-0.7	Omni

Table A8. Transmitting Antenna Gain

Transmit Antenna Gains			
Frequency(MHz)	Manufacturer	Gain (dBi)	Azimuth Pattern
440	Cushcraft	1.7	Omni
1360	Dorne&Margolin	11.3	Table Lookup
1920	Andrew	6.9	Omni

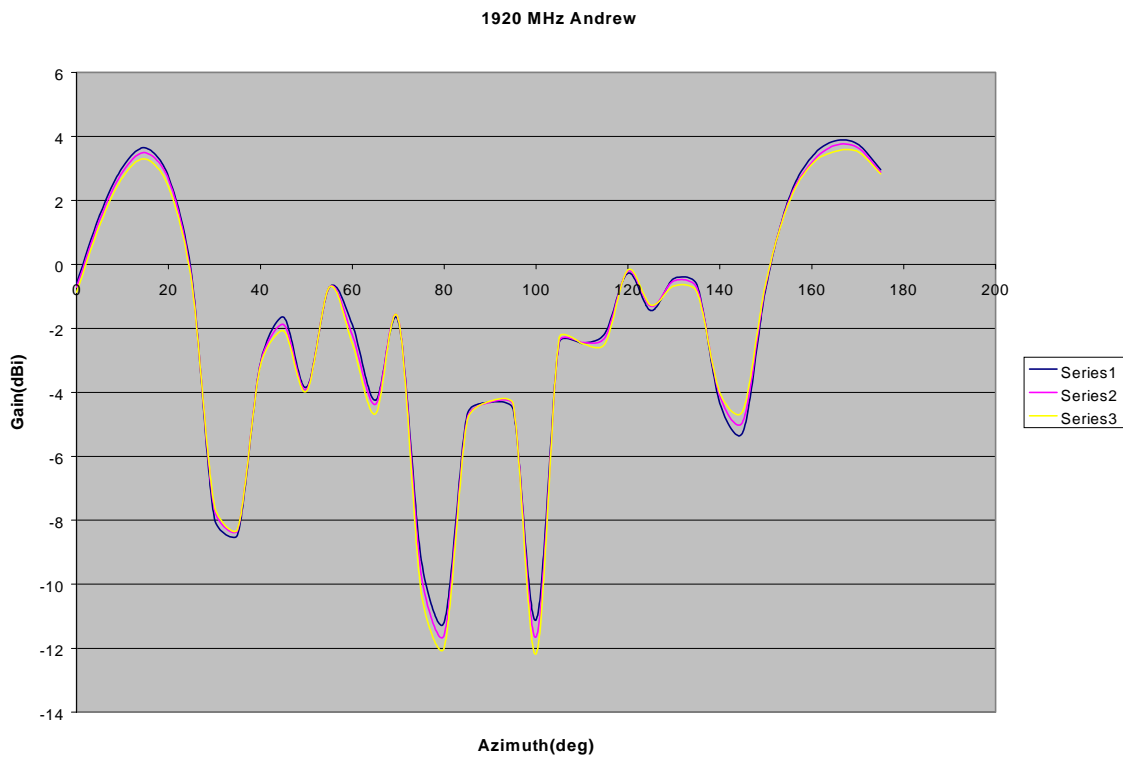


Figure A4. 1920 MHz Andrew receiving monopole (NIST Chamber).

APPENDIX B: EIRP AND ANTENNA GAINS

The transmitter effective isotropic radiated power (EIRP) is summarized in Table B1.

Table B1. EIRP Transmitted at EAFB

EAFB Cell 1 & Cell 2 Transmitter EIRP				
F(MHz)	P _{TX} (dBm)	Cable Loss(dB)	G _{TxAntenna} (dBi)	EIRP(dBm)
440	35.1	1.6	1.7	35.2
1360	35.0	4.0	11.3	42.3
1920	40.0	4.8	6.9	42.1

Table B2. Receiving Antenna Gains

Receive Antenna Gains			
Frequency(MHz)	Manufacturer	Gain (dBi)	Azimuth Pattern
440	Larson	1.2	Omni
1360	Larson	-1.3	Omni
1920	Andrew	-0.7	Omni

Table B3. Transmitter Antenna Gains

Transmit Antenna Gains			
Frequency(MHz)	Manufacturer	Gain (dBi)	Azimuth Pattern
440	Cushcraft	1.7	Omni
1360	Dorne&Margolin	11.3	Table Lookup
1920	Andrew	6.9	Omni